Physics of the Earth and Planetary Interiors 367 (2025) 107425

Contents lists available at ScienceDirect

Physics of the Earth and Planetary Interiors

journal homepage: www.elsevier.com/locate/pepi

Changbai intraplate volcanism and big mantle wedge

Dapeng Zhao [a,*], Genti Toyokuni [a], YoungHee Kim [b]

[a] Department of Geophysics, Graduate School of Science, Tohoku University, Sendai 980-8578, Japan
[b] Research Center for Deep-Surface Coupling of Earth, School of Earth and Environmental Sciences, Seoul National University, Seoul 08826, Republic of Korea

ARTICLE INFO

Keywords:
Changbai volcano
Big mantle wedge
Intraplate magmatism
Subduction zone
Seismic tomography
Seismic anisotropy
Deep earthquake

ABSTRACT

We review geophysical studies over the past two decades on the origin of the Changbai intraplate volcanism and the three-dimensional structure and geodynamics of the big mantle wedge (BMW) beneath NE Asia. Most studies have shown that the origin of the Changbai volcano (CBV) and other intraplate volcanoes in NE Asia is related to hot and wet upwelling flow in the BMW, located above the subducted Pacific slab that remains stagnant in the lower part of the mantle transition zone beneath East Asia. Fluids released from the Pacific slab through deep earthquake faulting provide additional magmas that feed the CBV, making it the largest and most active intraplate volcano in East Asia. Magma chambers have been identified in the crust and uppermost mantle under the CBV, forming a complex magmatic system. The CBV has the potential to erupt again in the (near) future; hence, continuous monitoring is essential to mitigate hazards. International cooperation is crucial for more effective studies of the CBV and BMW, particularly through the deployment of seismic stations in North Korea and the Japan Sea.

1. Introduction

The Changbai volcano (CBV) straddles the border between North Korea and China (Fig. 1a). This intraplate volcano has erupted several times in the past 2000 years (e.g., Simkin and Siebert, 1994) and was responsible for one of the largest eruptions in history, the Millennium Eruption of 946 CE (e.g., Xu et al., 2013; Hammond et al., 2020). An episode of unrest between 2002 and 2005, characterized by inflation and seismicity, brought attention back to this volcano (e.g., Xu et al., 2012; Liu et al., 2021). The magmatic process of continental intraplate volcanism is generally difficult to understand due to its complex interactions with the crust and the lithospheric mantle. The CBV has shown a complex history of eruptions and associated magmatic system (e.g., Simkin and Siebert, 1994; Liu, 1999; Liu, 2000). The origin of the CBV and the relationship between its crustal magmatic system and the upper mantle structure and processes are still debated issues, mainly due to the lack of tight and consistent geophysical constraints on the shallow and deep structures beneath NE Asia (e.g., Kim et al., 2017; Zhao, 2021). There are many Cenozoic volcanoes in the East Asia continent, but only a few are still active now, such as the Changbai and Wudalianchi volcanoes in NE China and the Tengchong volcano in SW China (Liu, 1999; Liu, 2000) (Fig. 1a). Among the intraplate volcanoes in East Asia, the CBV is the largest and most active one.

In the past two and a half decades, many researchers have used multidisciplinary approaches to investigate the crustal and upper mantle structures of the CBV and its adjacent areas. Early magnetotelluric soundings detected a high-conductivity layer in the crust under the volcano (Tang et al., 2001), and seismic explosion studies revealed low-velocity (low-V) anomalies in the crust and uppermost mantle under the volcano, which were inferred to reflect magma chambers (Zhang et al., 2002). Some early researchers considered the CBV to be a hotspot like Hawaii (e.g., Turcotte and Schubert, 1982), whereas others suggested that the formation of the intraplate volcanoes in NE Asia was associated with upwelling of hot asthenospheric materials as well as rift zones and fault zones in the continental lithosphere (e.g., Tatsumi et al., 1990; Foulger et al., 2005; Foulger, 2010).

Since early 1990s, many models of global seismic tomography have been developed, revealing the large-scale three-dimensional (3-D) mantle structure beneath western Pacific and East Asia (see Zhao, 2015 for a detailed review). One of such global tomographic models is shown in Fig. 2. It is visible that the subducting high-velocity (high-V) Pacific slab becomes flat in the mantle transition zone (MTZ, at 410–660 km depths) beneath the Korean Peninsula and East China, which is referred to as a stagnant slab (Fukao et al., 2001). Significant low-V anomalies appear above the stagnant slab, and they are overlain by active intraplate volcanoes such as the CBV and Wudalianchi volcano in NE China

* Corresponding author.
E-mail address: zhao@tohoku.ac.jp (D. Zhao).

https://doi.org/10.1016/j.pepi.2025.107425
Received 27 June 2025; Received in revised form 4 August 2025; Accepted 4 August 2025
Available online 6 August 2025

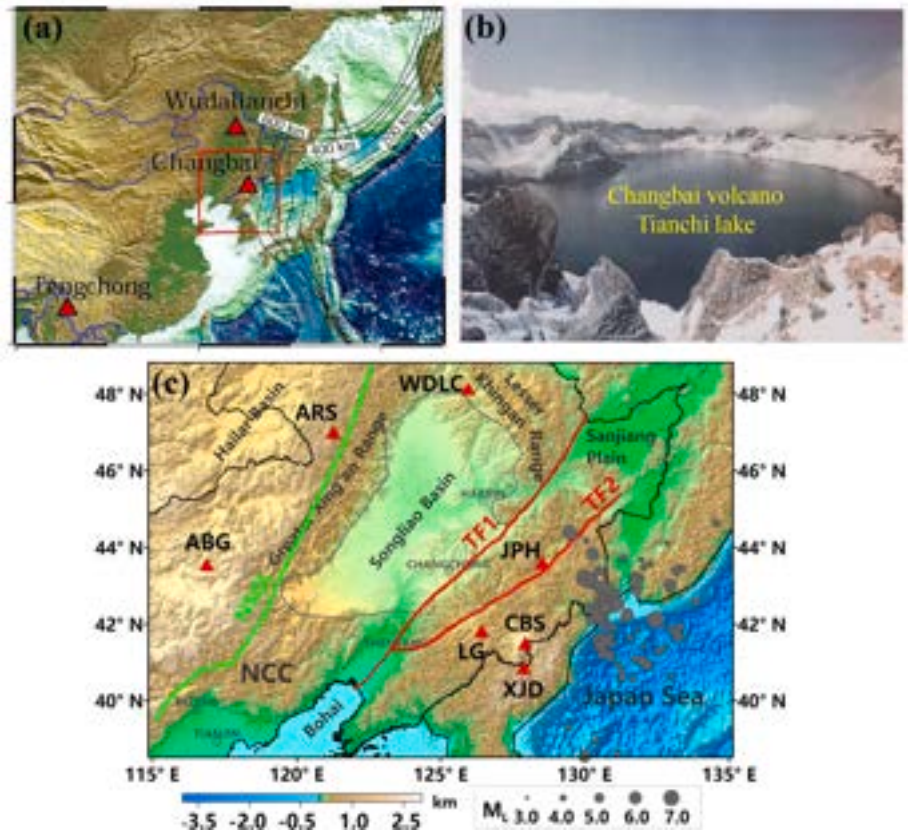

Fig. 1. (a) Map showing the surface topography of Western Pacific to East Asia (Zhao et al., 2009). Red triangles show the three active intraplate volcanoes (Wudalianchi, Changbai, and Tengchong). Dashed lines represent depth contours of the Wadati-Benioff seismic zone in the subducting Pacific slab. The red box outlines the area around the Changbai intraplate volcano (CBV). (b) A photo of the Tianchi lake atop the CBV (Liu, 1999). (c) Topography and tectonic background of Northeast Asia (Jia et al., 2022). The red triangles denote seven active intraplate volcanoes: CBS, Changbai; JPH, Jingpohu; LG, Longgang; ARS, Aershan; WDLC, Wudalianchi; ABG, Abaga; XJD, Xianjindao. NCC, the North China Craton. NSGL, the North–South gravity lineament. The gray dots denote deep earthquakes, whose magnitude scale is shown at the bottom. The red lines (TF1, TF2) show two branches of the Tanlu fault zone. The gray line shows the range of the Songliao Basin. The small circles denote locations of major cities (Harbin, Changchun, Shenyang, Beijing and Tianjin). (For interpretation of the references to colour in this figure legend, the reader is referred to the web version of this article.)

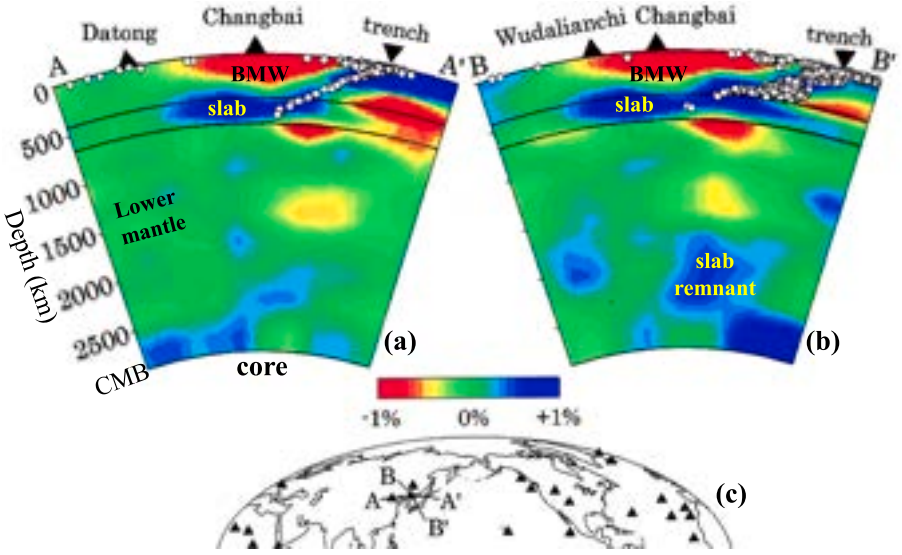

Fig. 2. (a, b) Vertical cross-sections of whole-mantle P-wave velocity (Vp) tomography. Red and blue colors denote low and high Vp perturbations (in %), respectively, relative to the 1-D iasp91 Earth model. The scale bar for Vp perturbations is shown below the cross-sections. White dots mark seismicity within a 150 km width of each profile. The two solid lines indicate the 410 and 660 km discontinuities. Solid triangles denote intraplate volcanoes, while inverted triangles indicate the location of the Japan Trench. CMB, the core-mantle boundary. (c) Map showing the locations of the two cross-sections in (a) and (b). Triangles denote hotspots or intraplate volcanoes on Earth. Modified from Zhao (2004). (For interpretation of the references to colour in this figure legend, the reader is referred to the web version of this article.)

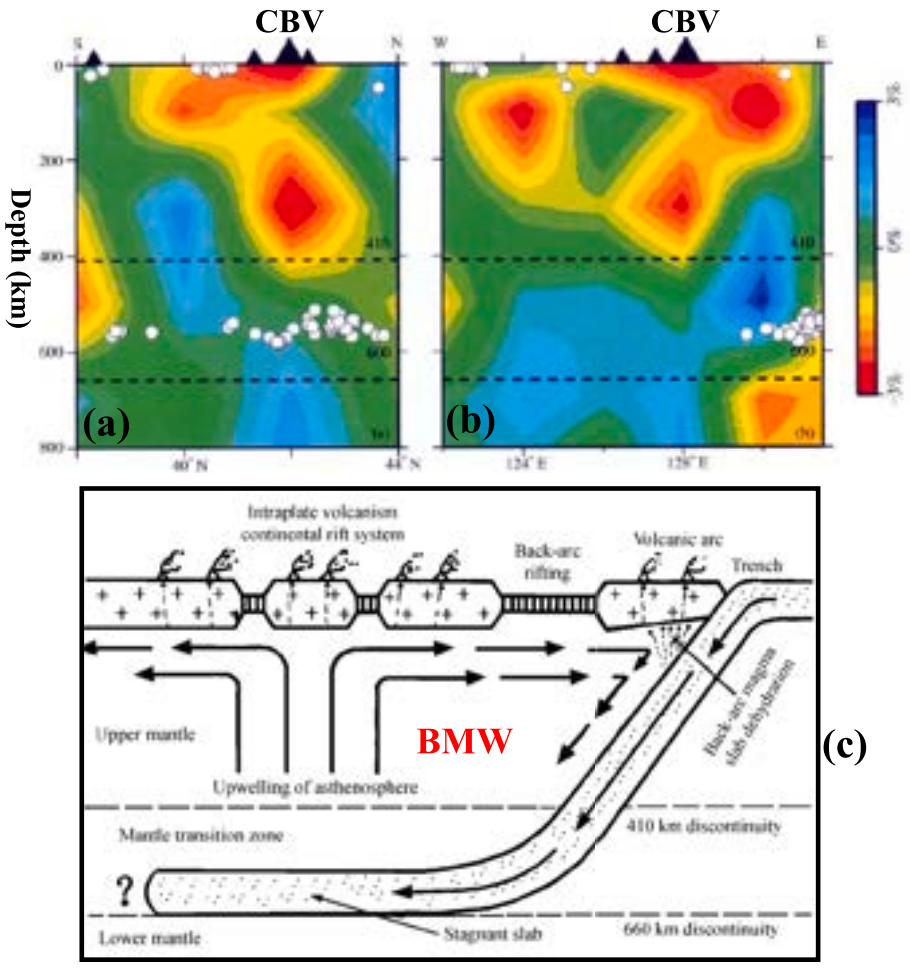

Fig. 3. (a) North-south and (b) east-west vertical cross-sections of Vp tomography beneath the Changbai intraplate volcano (CBV). Red and blue colors denote low and high Vp perturbations, respectively, whose scale is shown on the right. Black triangles denote intraplate volcanoes. White dots show local seismicity within a 200 km width of each profile. Two dashed lines denote the 410 and 660 km discontinuities. (c) Schematic east-west vertical cross-section illustrating the upper-mantle structure and geodynamics beneath NE Asia. The subducting Pacific slab becomes stagnant in the mantle transition zone, forming a big mantle wedge (BMW) above it. Convective circulation within the BMW and deep dehydration reactions of the subducted slab generate hot and wet asthenospheric upwelling, leading to the back-arc rifting, the Japan Sea opening, and the intraplate volcanoes in NE Asia. Modified from Zhao et al. (2004). (For interpretation of the references to colour in this figure legend, the reader is referred to the web version of this article.)

(Fig. 2b). High-V anomalies are also visible in the lower mantle, even down to the core-mantle boundary (CMB), which may reflect the slab remnants, because the subducted slab collapses intermittently down to the CMB due to gravity instability (e.g., Maruyama, 1994; Zhao, 2004; Toyokuni et al., 2022).

Zhao et al. (2004) first applied teleseismic tomography to investigate the local 3-D P-wave velocity (Vp) structure of the upper mantle beneath the CBV (Fig. 3a,b). A clear low-V anomaly was detected under the CBV from the surface to 410 km depth, and a high-V anomaly was revealed in the MTZ where deep earthquakes occurred. On the basis of the results of global tomography (Fig. 2) and local tomography (Fig. 3), Zhao et al. (2004) proposed a so-called big mantle wedge (BMW) model (Fig. 3c). They suggested that a BMW has formed above the stagnant Pacific slab beneath East Asia, and due to abundant fluids from the slab dehydration and corner flows in the BMW, hot and wet upwelling flows are produced in the BMW, which penetrate through the continental lithosphere to the surface, causing the Japan Sea opening, back-arc spreading, and the intraplate volcanoes in East Asia such as the CBV. This BMW concept was further confirmed and strengthened by subsequent tomographic studies (Lei and Zhao, 2005; Zhao et al., 2007, 2009).

In the past two decades, a great number of researchers have examined this BMW model and used it to investigate the origins of CBV and other intraplate volcanoes in East Asia by taking various geophysical, geochemical and geological approaches. Thanks to these multidisciplinary studies, there have been great advances in our understanding of the origin of the intraplate volcanism, as well as the detailed structure and processes of the BMW in NE Asia. In this article, we review these studies with a focus on the geophysical findings. For the related geological and geochemical studies, the reader is referred to comprehensive reviews by Zhang et al. (2018), Xu et al. (2018) and Tang et al. (2023).

2. Seismic tomography and BMW in East Asia

An important breakthrough in understanding of the 3-D mantle structure of East Asia was made by Huang and Zhao (2006), who used about one million P-wave arrival times of local and regional earthquakes to determine high-resolution Vp tomography of the crust and mantle down to 1300 km depth beneath East Asia. The subducting Pacific slab and the stagnant slab in the MTZ were clearly revealed, and intermediate-depth and deep earthquakes were observed to occur down to ~600 km depth within the slab (Fig. 4). Low-V anomalies are visible in the BMW beneath the Japan Sea, the CBV and its surrounding areas, as well as in the upper mantle and the MTZ under the intraplate Datong volcano (Fig. 4).

Fig. 5a shows the surface topography of East Asia. Fig. 5b shows the

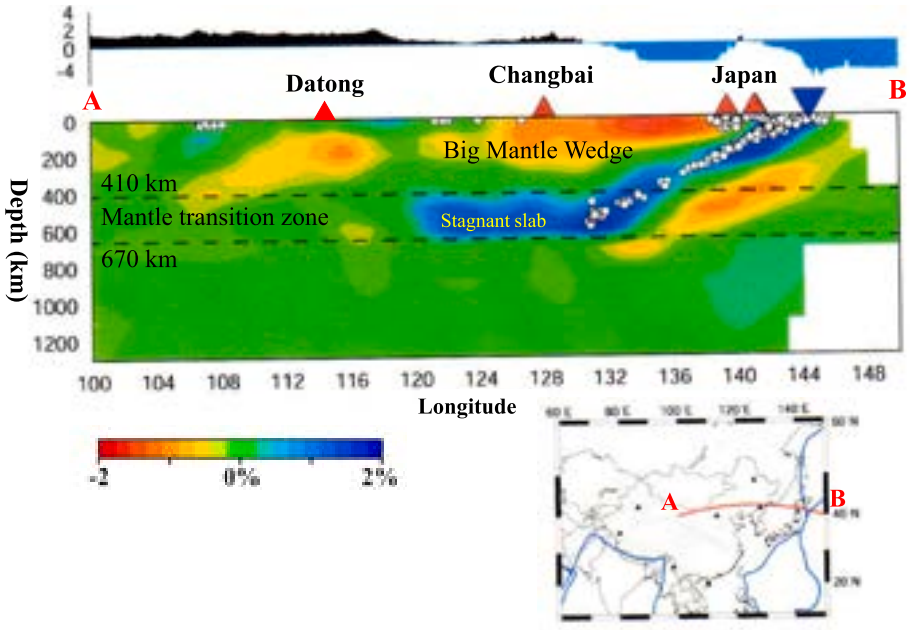

Fig. 4. East-west vertical cross-section of regional Vp tomography extending from the surface to a depth of 1300 km along the profile indicated on the inset map (Huang and Zhao, 2006). Red and blue colors denote low and high Vp perturbations, respectively, relative to the 1-D iasp91 Earth model. The Vp perturbation scale is shown at the bottom. White dots denote earthquakes within a 100 km width of the profile. The two dashed lines show the 410 and 670 km discontinuities. Red and black triangles mark active volcanoes, while the inverted blue triangle indicates the location of the Japan Trench. The surface topography along the profile is shown above the tomographic image. Blue lines on the inset map denote major plate boundaries. (For interpretation of the references to colour in this figure legend, the reader is referred to the web version of this article.)

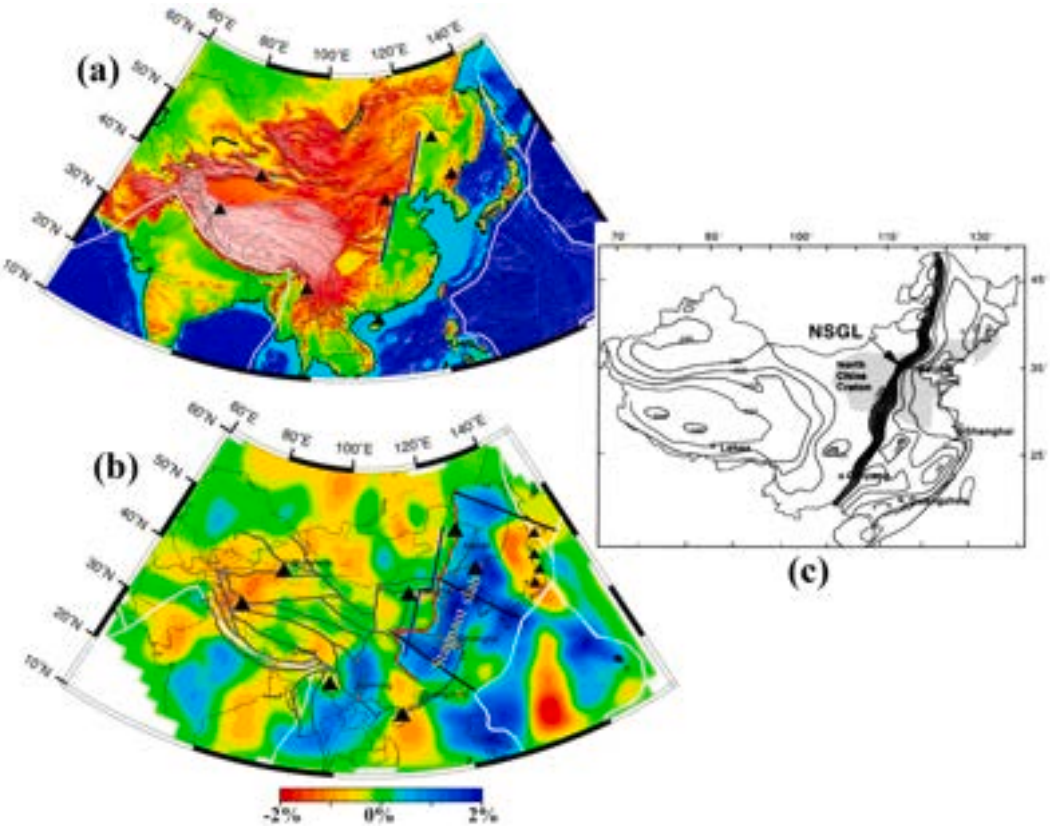

Fig. 5. (a) Surface topography of East Asia and (b) tomographic image at 600 km depth (Huang and Zhao, 2006). The blue line denotes a surface topographic boundary. The red curved line in (b) denotes the western edge of the stagnant Pacific slab in the mantle transition zone. The white lines denote major plate boundaries on the surface. (c) Distribution of the Bouguer gravity anomalies in China (Ma, 1989; Xu, 2007). The bold line denotes the north-south gravity lineament (NSGL). The gray patch denotes the North China Craton. (For interpretation of the references to colour in this figure legend, the reader is referred to the web version of this article.)

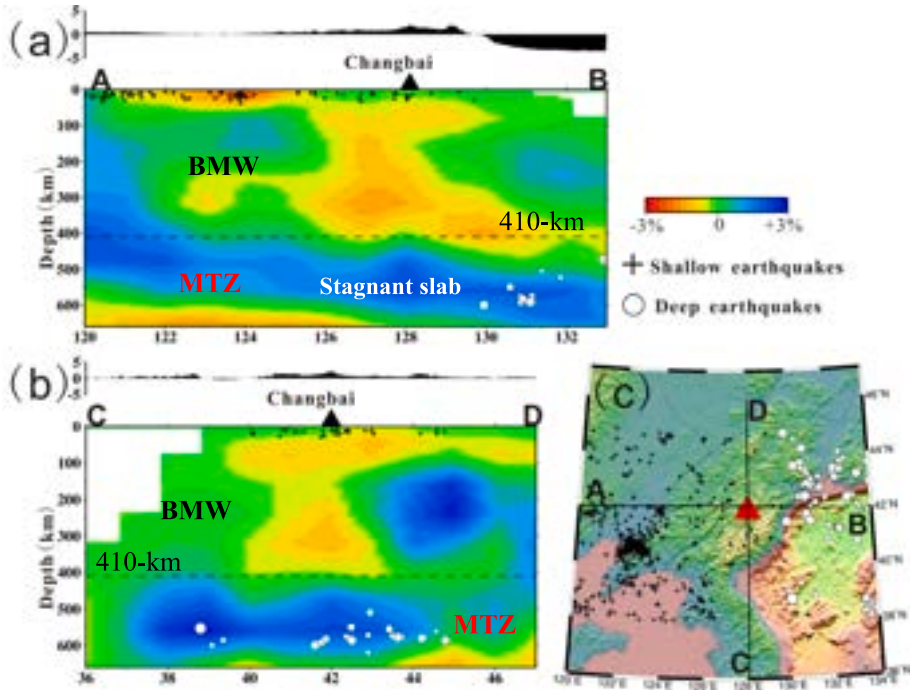

Fig. 6. (a) East-west and (b) north-south vertical cross-sections of local Vp tomography along the profiles shown in (c). Red and blue colors denote low and high Vp perturbations, respectively, whose scale is shown beside (a). The black triangle denotes the active Changbai volcano. The dashed line shows the 410 km discontinuity. (c) Map showing locations of the two cross-sections in (a) and (b). The red triangle denotes the Changbai volcano. Black crosses and white dots show shallow (0–30 km depths) and deep-focus (450–600 km) earthquakes, respectively. Modified from Zhao et al. (2009). (For interpretation of the references to colour in this figure legend, the reader is referred to the web version of this article.)

Vp tomography at 600 km depth, where the stagnant Pacific slab is clearly visible. The western edge of the stagnant slab roughly coincides with a surface topographic boundary in East China (Fig. 5a,b), which also corresponds to a gravity anomaly boundary known as the north-south gravity lineament (NSGL, Fig. 5c). The NSGL extends over 4000 km from Russia to South China, which is characterized by an abrupt change in the observed Bouguer gravity anomaly, ranging from −100 mGal in the west to −40 mGal in the east over a distance of <100 km (Ma, 1989; Xu, 2007; Deng et al., 2021). These results indicate that the northwestward subducting Pacific slab has reached the NSGL, suggesting that the NSGL likely represents the western edge of the BMW (Zhao et al., 2007; Deng et al., 2021; Jia et al., 2022). It is also clear that the structures and geodynamic processes in and around the MTZ and BMW have significantly affected surface geology and tectonics in East Asia (Huang and Zhao, 2006; Zhao, 2021).

Zhao et al. (2009) determined an even higher Vp tomographic model of the crust and upper mantle beneath NE Asia by jointly inverting a large dataset of arrival times of both local and teleseismic earthquakes. They revealed a prominent low-V anomaly in the crust and upper mantle down to ~410 km depth beneath the CBV (Fig. 6). A broad high-V anomaly appears in the MTZ where deep earthquakes occurred actively, indicating that the stagnant Pacific slab does exist under the CBV. These findings provide strong support for the BMW model and suggest that the CBV magmatism and volcanism are driven by the upwelling of hot and wet asthenospheric materials in the BMW. Hence, the CBV is not a hotspot related to a deep mantle plume, but rather caused by plate tectonic processes in the upper mantle and the MTZ (Zhao et al., 2004; Lei and Zhao, 2005).

Subsequent studies of large-scale regional tomography have not only confirmed the above-mentioned main features of the mantle structure beneath East Asia but also revealed finer-scale details (e.g., Wei et al., 2012, 2015, 2019; Ma et al., 2018, 2019). Lateral velocity variations were also revealed within the subducting Pacific slab and the stagnant slab in the MTZ (see Figs. 4, 5b, 6 and 7, as well tomographic images that are introduced in the next section), which may be caused by several factors, such as changes in slab age, compositional heterogeneity, the presence of oceanic fracture zones in the Paleo-Pacific lithosphere, and subslab hot upwelling flows, etc. (Zhao et al., 1992, 2012; Huang et al., 2013; Asamori and Zhao, 2015; Liu et al., 2017; Fan and Zhao, 2021; Toyokuni et al., 2025; Hu et al., 2023; Toyokuni and Zhao, 2024; Wang et al., 2025).

P-wave anisotropic tomography of NE Asia (Wei et al., 2015) revealed that the dominant fast velocity direction (FVD) of azimuthal anisotropy in the BMW is NW-SE, roughly parallel with the subduction direction of the Pacific plate, which reflects the general direction of mantle flow in the BMW driven by the Pacific slab subduction (Fig. 7). Jia et al. (2022) determined Vp anisotropic tomography beneath NE China. In the upper crust, nearly E-W FVDs were revealed in the central Songliao Basin (see Fig. 1c), which is surrounded by circular-shaped FVDs along the basin's edges. The E-W FVDs may reflect microcracks or fractures in the upper crust, which are aligned under the control of regional tectonic stress. In the lower crust, low-V anomalies with NE-SW FVDs were detected along the Tanlu fault zone (see Fig. 1c), potentially indicating NE-SW trending ductile deformation or viscous flow along the fault zone. The FVDs are mainly NNW-SSE to N-S in the uppermost mantle beneath most of NE China, which may reflect fossil deformation of the mantle lithosphere caused by the Paleo-Pacific plate subduction. High-V anomalies with NE-SW FVDs were revealed at ~100 km depth directly beneath the Great XingAn Range in the northern part of NE China, which may reflect an old lithospheric remnant. In the deep upper mantle, the FVDs are mostly NW-SE (Fig. 7), consistent with the results of Wei et al. (2015) and SKS wave splitting measurements (e.g., Lu et al., 2020; Gao et al., 2024), which reflect convective flows in the BMW. Note that SKS wave denotes a seismic wave that propagates as a P-wave in the outer core but as an S-wave in the crust and mantle.

In addition to the above-mentioned tomographic studies, teleseismic receiver-function studies have revealed localized depth variations of the 410 and 660 km discontinuities (e.g., Li and Yuan, 2003; Lee et al., 2014;

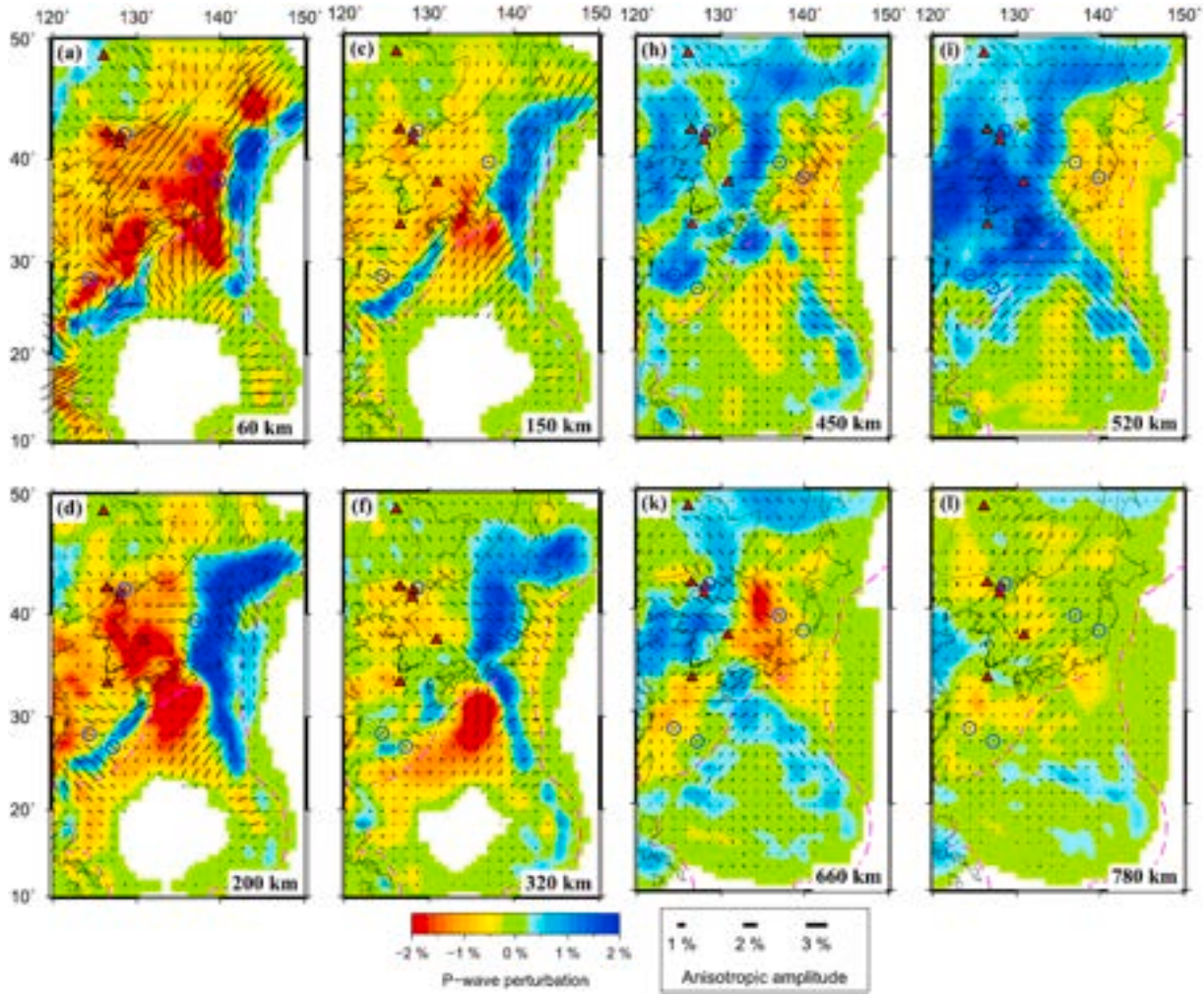

Fig. 7. Map views of Vp anisotropic tomography at different depths. The layer depth is shown at the lower-right corner of each map. The red and blue colors denote low and high isotropic Vp perturbations, respectively. The azimuth and length of each black bar represent the fast-velocity direction and amplitude, respectively, of Vp azimuthal anisotropy. The scales for the isotropic Vp perturbation and anisotropic amplitude are shown at the bottom. The red triangles denote active intraplate volcanoes. The dashed purple lines denote plate boundaries at the surface. The five open circles denote locations where azimuthal distributions of P-wave rays were examined by the authors. Modified from Wei et al. (2015). (For interpretation of the references to colour in this figure legend, the reader is referred to the web version of this article.)

Tian et al., 2016). SS precursors and triplicated phases associated with the MTZ discontinuities were also used to investigate the thickness and geophysical properties of the stagnant slab (e.g., Tajima et al., 2009; Ye et al., 2011; Gu et al., 2012; Li et al., 2013; Dokht et al., 2016; Han et al., 2021). Numerical modeling studies suggested that the intraplate volcanism in NE Asia could be explained by hot and wet upwelling flows associated with the slab rollback, trench retreat, and interaction of the slab with a hydrous MTZ (e.g., Richard and Iwamori, 2010; Kameyama and Nishioka, 2012; He, 2014, 2017; Yang and Faccenda, 2020; Dasgupta and Lee, 2025). All these results support the BMW model.

3. Deep earthquakes and Changbai volcanism

Intermediate-depth and deep-focus earthquakes frequently occur in NE Asia, forming a well-defined Wadati-Benioff deep seismic zone within the subducting Pacific slab (Figs. 8 and 9). Some of the deep events are quite large, with magnitudes greater than 7.0. Two large deep earthquakes occurred in recent years close to the CBV. One event (Mw 7.1) took place on April 8, 1999 at a depth of 575.4 km. The other (Mw 7.2) happened on June 29, 2002 at 581.5 km depth (Fig. 8). The epicenters of both events are located ~300 km to the northeast of the CBV. This distance is about half of their focal depths (> 575 km). A few other large deep earthquakes (>M 7.0) occurred in the same area in the past 50 years, including an M7.2 event in 1977 and an M7.6 event in 1994 (Zhao and Tian, 2013).

Fig. 10 shows five vertical cross-sections of Vp tomography passing through the CBV, and Fig. 11 shows map views of the Vp tomography in the deep upper mantle beneath NE Asia (Zhao and Tian, 2013). In addition to the features as mentioned above (Fig. 6), we can see that, in the asthenosphere (~300–410 km depths), the low-V anomaly under the CBV extends towards the Japan Sea side and reaches over a swarm of deep earthquakes in the subducting Pacific slab (Figs. 10 and 11). On the basis of the seismological results (Figs. 8–11) and integrating all the geophysical, geochemical and petrologic findings, Zhao and Tian (2013) proposed that there is a close relationship between the Changbai volcanism and deep earthquakes in the Pacific slab (Fig. 12). Previous studies have shown that large shallow earthquakes occurred frequently in the Pacific Plate beneath the outer-rise area close to the Japan Trench (Fig. 8; Kanamori, 1971; Obana et al., 2012; Lay et al., 2013; Kubota et al., 2019), and seawater may enter down to a deep portion of the oceanic lithosphere through the active normal faults whose ruptures generated the large outer-rise earthquakes. Seawater or fluids could be preserved within the active faults in the oceanic lithosphere even after the Pacific Plate subducts into the mantle. Among the many large deep

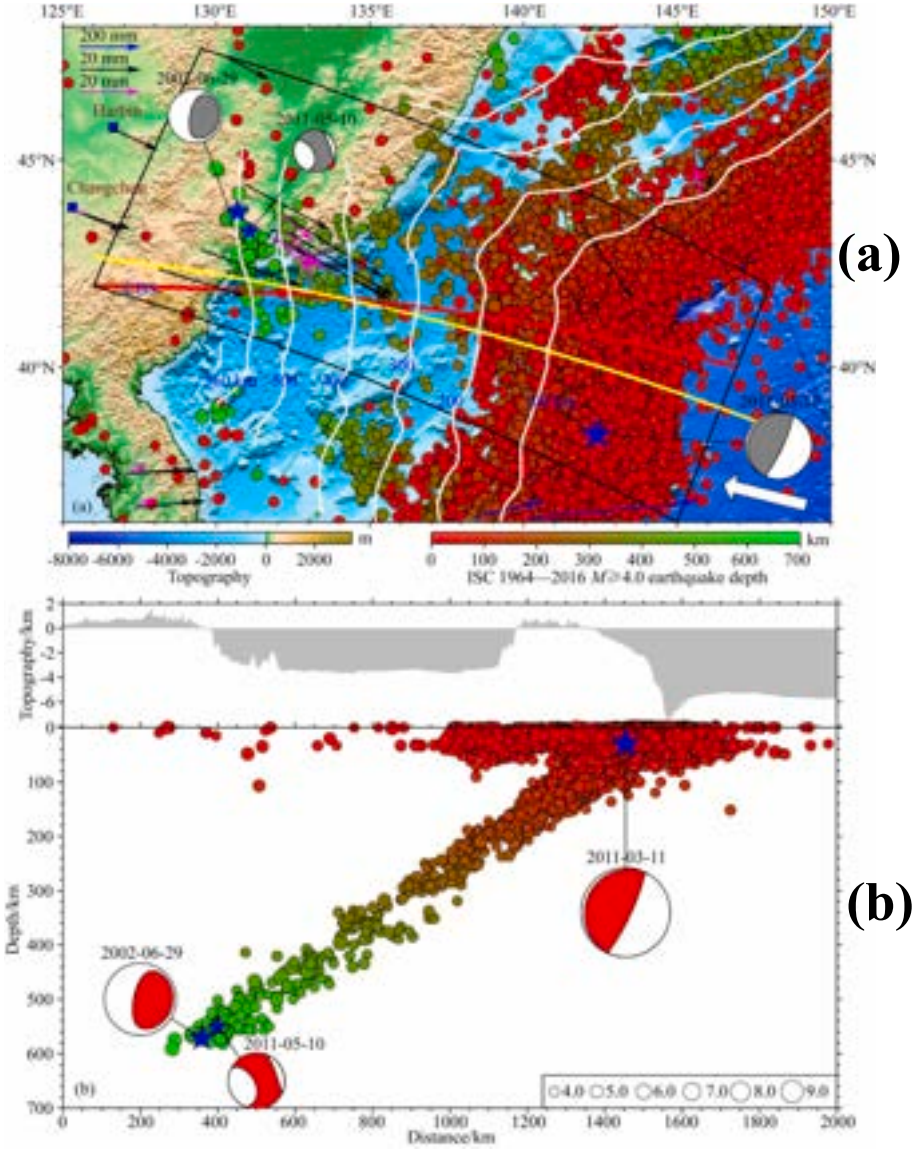

Fig. 8. (a) Seismicity (M ≥ 4.0) during 1964–2016 compiled by the International Seismological Center. The dot colors denote focal depths whose scale is shown below (a). The white contours denote depths to the Pacific slab upper boundary (Hayes et al., 2012). The bold white arrow denotes the subduction direction of the Pacific plate. The thin color arrows denote GPS observation results. (b) Vertical cross-section showing earthquakes within a 300 km width of the profile as shown in the yellow line in (a). The gray and red beach balls denote focal mechanism solutions of the Tohoku megathrust earthquake (Mw 9.0) on March 11, 2011 and two deep earthquakes (M7.2, M6.1) on June 29, 2002 and May 10, 2011, whose epicenters and hypocenters are shown in blue stars in (a) and (b), respectively. After Chen et al. (2021). (For interpretation of the references to colour in this figure legend, the reader is referred to the web version of this article.)

earthquakes in the subducting Pacific slab under the Japan Sea and the East Asian margin (Figs. 8–11), at least some of them were caused by reactivation of the faults preserved in the subducting slab, and the fluids preserved in the faults within the slab may cause non-double-couple components of the deep earthquake faulting (Zhao and Tian, 2013). Fluids preserved in the slab may be released to the overlying BMW through faulting processes of the large deep earthquakes (Fig. 12). Because large deep events occur frequently in the vicinity of the CBV, more fluids could be supplied to this volcano than in other areas in NE Asia, making Changbai the largest and most active intraplate volcano in the region.

Note that another swarm of deep events occurred to the east of the Ulleung intraplate volcano under the Japan Sea, but there is no low-V anomaly under the volcano (Figs. 10e and 11). This is because Ulleung is located at the southeastern edge of the Vp tomographic model, and there is no seismic station in the Japan Sea. Thus, the Vp tomography has no resolution under Ulleung; even if a low-V anomaly exists there, it could not be imaged by this Vp tomography (Zhao et al., 2009; Zhao and Tian, 2013). A regional S-wave velocity (Vs) tomography of NE Asia revealed a continuous low-Vs anomaly at depths of 0–400 km beneath the Ulleung volcano, which was interpreted as upwelling flow from the Pacific slab at 400 km depth, possibly related to fluids (Simute et al., 2016). However, this Vs tomography could not resolve the subducting Pacific slab well, in particular, the slab in the MTZ. Taking into account the distribution of large deep earthquakes (Figs. 10 and 11) and the Vs tomography (Simute et al., 2016), we suggest that the formation of the Ulleung volcano might be also affected by fluids from the Pacific slab through faulting processes of its nearby deep earthquakes (Fig. 11b,c).

Using the teleseismic receiver-function method, Tian et al. (2016) investigated the detailed MTZ structure beneath the CBV. They revealed significant depth variations of the 410, 520 and 660 km discontinuities (Fig. 13). Under the CBV, a broad depression of the 410 km discontinuity was detected where a low-V anomaly exists, which may reflect large-

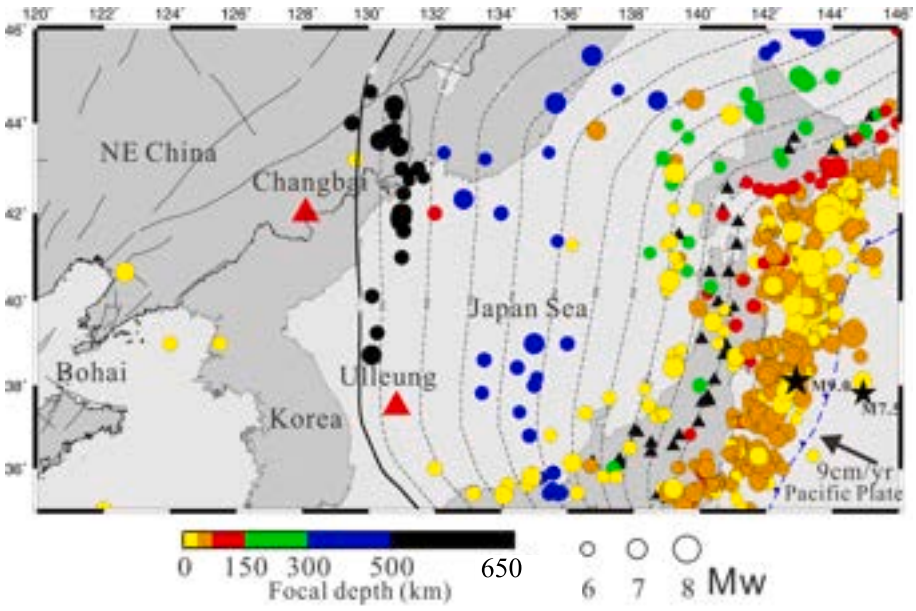

Fig. 9. Tectonic framework of NE Asia. The color dots show epicenters of large earthquakes (M ≥ 6.0) that occurred between 5 January 1900 and 30 September 2009, compiled by the International Seismological Center. The dot size and color denote the earthquake magnitude and focal depth, respectively, whose scales are shown at the bottom. The black stars denote the great Tohoku-oki earthquake (Mw 9.0) and an outer-rise earthquake (Mw 7.5) which occurred on 11 March 2011. The contour lines show depths to the upper boundary of the subducting Pacific slab. The blue sawtooth line denotes the Japan Trench. The red triangles denote active Changbai and Ulleung intraplate volcanoes. The black triangles denote active arc volcanoes on the Japan Islands. The thin black lines denote major active faults. After Zhao and Tian (2013). (For interpretation of the references to colour in this figure legend, the reader is referred to the web version of this article.)

scale hot mantle upwelling around the 410 km discontinuity with a positive Clapeyron slope. The 520 km discontinuity was also identified clearly, and its uplift occurs above the stagnant Pacific slab. The 660 km discontinuity exhibits a prominent depression, which is elongated along the trend of the deep earthquake swarm, and the depression area has a lateral extent of ~400 km (Fig. 13). Because the 520 and 660 km discontinuities correspond to positive and negative Clapeyron slopes, respectively, this result suggests that the uplift of the 520 and the depression of the 660 are caused by the cold stagnant slab (Tian et al., 2016).

Continuous monitoring of the CBV by means of volcanic seismicity, ground deformation, and volcanic gas geochemistry has yielded robust evidence for magmatic unrest of the volcano during July 2002 to July 2005 (Xu et al., 2012; Liu et al., 2021). During this active period, the frequency of volcanic earthquakes increased by about two orders of magnitude compared to that of the background inactive periods (Fig. 14). The active period was also accompanied by ground inflation, high values of CO_2, He, H_2, and high ratios of N_2/O_2 and $^3He/^4He$ in volcanic gases released from three hot springs near the caldera rim. The monitoring evidence implies pressurization of the magma chamber, possibly caused by incremental magma recharge. The ground deformation data from both GPS and precise leveling were modeled to suggest the corresponding deformation source at 2–60 km depths beneath the CBV summit, where earthquake swarms were detected in 2002 and 2003. These results suggest that the magma chamber beneath the CBV has awakened and resumed activity after remaining dormant since 1903 CE (Xu et al., 2012). Liu et al. (2021) performed systematic detection of microseismic events recorded at a seismic station near the CBV from July 1999 to July 2007 (Fig. 14). They detected 3763 volcano-tectonic (VT) events and some long-period (LP) and harmonic-spectra (HS) events between July 2002 and July 2007. The intense VT activity along with recurring LP and HS events, as well as other geodetic and geochemical evidence, suggest magma movement during the CBV unrest. Taking into account the link between the deep earthquakes and CBV proposed by Zhao and Tian (2013) (Fig. 12), Liu et al. (2021) suggested a delayed-triggering relationship between the 2002 M7.2 deep earthquake and the CBV unrest (Figs. 14a and 15). The small magnitudes of the VT events and the limited numbers of LP and HS events suggest that the 2002 M7.2 deep earthquake triggered CO_2-rich bubble excitation in the mid-crust magma system, resulting in overpressure and a small magma injection into the shallow magma chamber at ~5 km depth, leading to the 2002–2005 CBV unrest (Fig. 15). These results support the proposal of Zhao and Tian (2013) that the CBV magmatism is related to the frequent occurrence of large deep earthquakes (M > 7.0) whose ruptures release fluids preserved within the subducting slab to the overlying BMW, producing more magmas feeding the CBV.

4. BMW structures and geodynamics

Since the BMW hypothesis was first proposed (Zhao et al., 2004; Lei and Zhao, 2005), many versions of the BMW model have been published based on various geoscientific results and approaches. Some of the BMW models are shown in Figs. 16–18, which are briefly introduced here, roughly in a temporal order.

Using broadband body-wave seismograms of three deep earthquakes near the Russia–China border, Li et al. (2013) investigated Vp and Vs structures of the MTZ beneath NE China (Fig. 16a). Their results show that the high-V stagnant Pacific slab has a thickness of ~140 ± 20 km, lying above a slightly depressed 660 km discontinuity, and that there is a Vs reduction of ~2.5 % in the deeper part of the MTZ. Overall, the MTZ is featured by low Vs and high Vp/Vs ratio. A water-rich MTZ with 0.2–0.4 wt% of H_2O may account for the discrepancy between the observed Vp and Vs structures, which supports a mineral physics result (Kuritani et al., 2011). These results suggest a scenario of a viscosity-dominated stagnant slab with an increased thickness of ~140 km, caused by the large viscosity contrast between the lower and upper mantles. The addition of water and eastward trench retreat might facilitate stagnation of the Pacific slab beneath NE Asia.

The CBV has long been regarded as a significant source of carbon released by its episodic eruptions since the Quaternary and magma-related geothermal activities at present (e.g., hot springs and soil micro-seepage). Zhang et al. (2015) measured soil CO_2 flux of the CBV

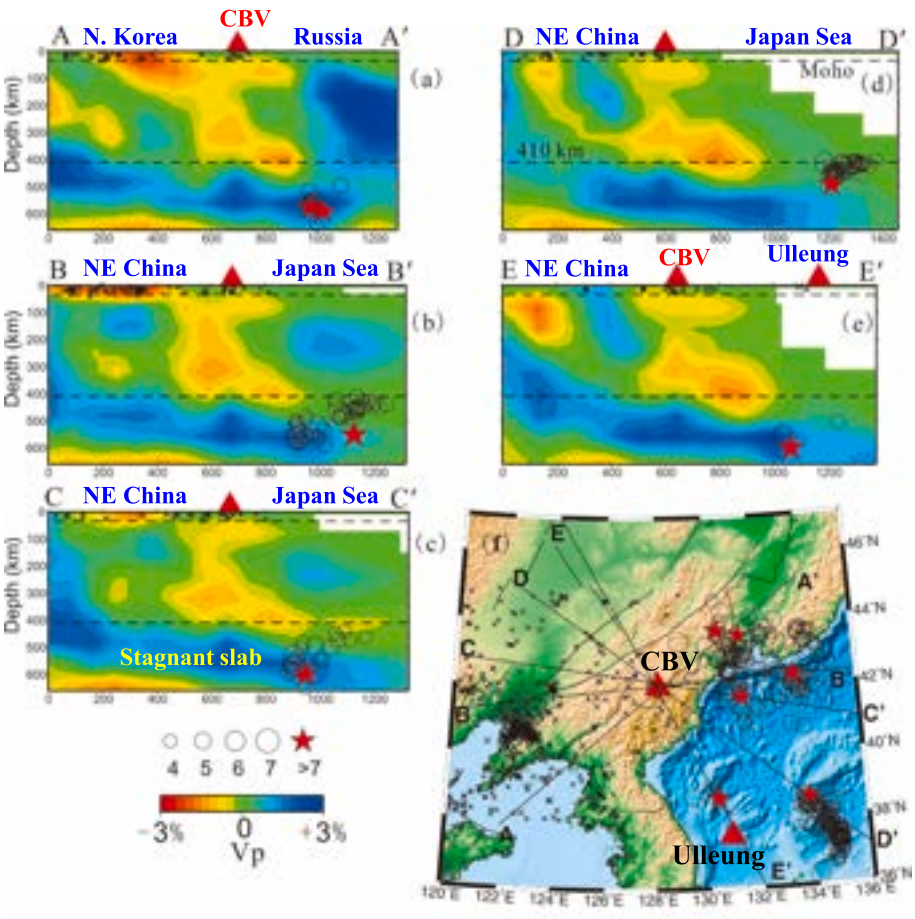

Fig. 10. (a-e) Vertical cross-sections of local Vp tomography along the profiles shown on the inset map (f). Blue and red colors denote high and low Vp perturbations, respectively. The cross symbols denote crustal earthquakes. Deep earthquakes are shown as open circles ($M < 7.0$) and red stars ($M \geq 7.0$). The Vp perturbation and earthquake magnitude scales are shown below (c). The two dashed lines denote the Moho and 410 km discontinuities. After Zhao and Tian (2013). (For interpretation of the references to colour in this figure legend, the reader is referred to the web version of this article.)

and suggested that the upper mantle, slab carbonate and organic metasediments from both the subducted Pacific slab and the overriding continental crust were involved in the origin and evolution of the Changbai volcanic gases. Combining the geochemical and geophysical results, they proposed that CO_2-rich volcanic gases released by the CBV might originate from the stagnant Pacific slab in the MTZ (Fig. 16b). The MTZ-derived volatiles, mixed by components from the upper mantle, slab carbonate and subducted organic metasediments, underwent variable degrees of contamination by organic metasediments in the continental crust during transport from a magma chamber to the surface. The slab-derived materials contribute over half of the total carbon inventory at the CBV, suggesting the significance of carbonatitic and carbonated silicate melts on liberating carbon from the Earth's interior to the exosphere.

Choi et al. (2017) estimated the major and trace element concentrations of olivine-hosted melt inclusions in basalts from the CBV. They suggested that the intraplate volcanism in NE Asia is closely associated with the flat Pacific slab in the MTZ, which generates a wet plume (Fig. 16c). Thermal decomposition of K-hollandite within recycled continent-derived sediments is likely to metasomatize the ambient mantle peridotite above the flat slab. As the plume ascends through the upper mantle, the metasomatized mantle and recycled oceanic crustal materials entrained by the plume may undergo partial melting, resulting in the Changbai volcanism (Kuritani et al., 2011; Choi et al., 2017).

The Circum-Pacific subduction zone is a well-known gold metallogenic domain in the world, with two important gold metallogenic provinces, the North China Craton and Nevada, which are related to the destruction of the North China Craton (e.g., Tian and Zhao, 2013; Guo et al., 2024) and the Wyoming Craton (e.g., Zhao et al., 2024a), respectively. Zhu and Sun (2021) suggested that the ore-forming fluids were derived from the stagnant slab in the MTZ (Fig. 16d). The oceanic lithosphere usually contains a serpentine layer up to a few km thick. During the plate subduction, serpentine is dehydrated at ~300 km depth. The overlying BMW is hydrated during the breakdown of these hydrous facies in the MTZ. The slab dehydration in the MTZ releases sulfur-rich fluid, which extracts gold and other chalcophile elements in the surrounding rocks, forming gold-rich fluid. The fluid induces metasomatism and forms pargasite and other water-bearing minerals when it migrates upward to the cratonic lithosphere, resulting in a water- and gold-rich weak layer. During the craton destruction, the weak layer becomes destabilized, releasing gold-bearing fluids that accelerate the destruction. The ore-forming fluids migrate along the shallow weak zone and are accumulated at shallow depths, and subsequently escape along deep faults during major tectonic events, leading to explosive gold mineralization (Zhu and Sun, 2021).

Deng et al. (2021) conducted gravity modeling to investigate relative contributions of the thickness and composition of the crust and upper mantle as well as the stagnant slab in the MTZ to the observed gravity anomaly in and around the NSGL (Figs. 5c and 17a). They showed that the crustal thickness was the dominant factor in the NSGL formation, with lithospheric composition also playing a role. Lateral variations in the lithospheric mantle composition and crustal/lithospheric thickness across the NSGL could cause lithospheric thinning and mantle replacement in the eastern part of the North China Craton during the late

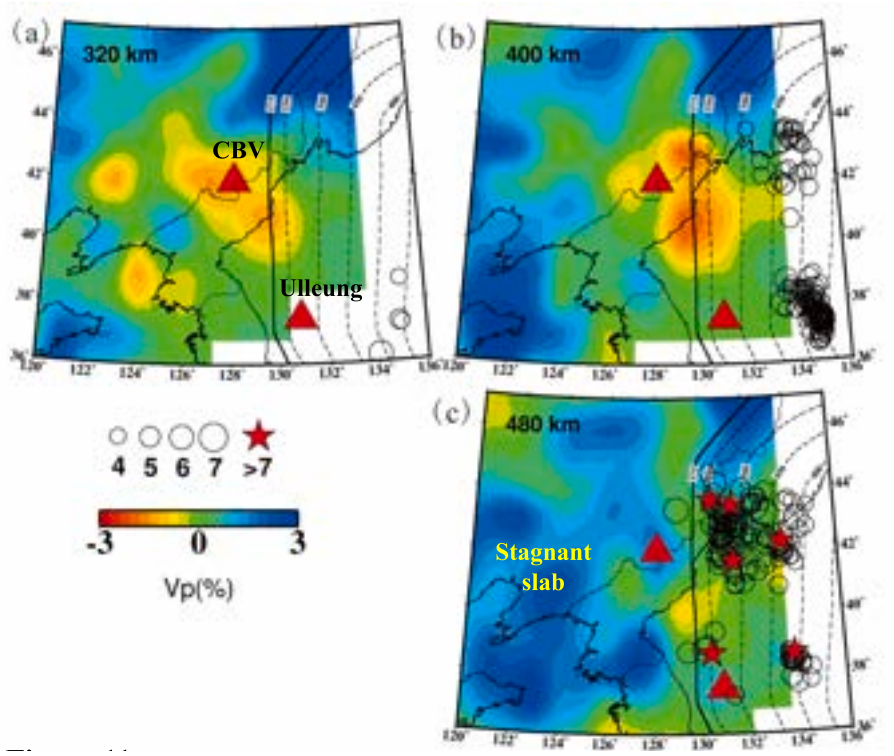

Fig. 11. Map views of local Vp tomography at (a) 320, (b) 400 and (c) 480 km depths. Blue and red colors denote high and low Vp perturbations, respectively. Deep earthquakes (>350 km depth) that occurred during 1964–2009 within a depth range of 40 km of each layer are shown in open circles ($M < 7.0$) and red stars ($M \geq 7.0$). The Vp perturbation and earthquake magnitude scales are shown below (a). The red triangles denote the Changbai and Ulleung intraplate volcanoes. The contour lines show depths to the upper boundary of the subducting Pacific slab. After Zhao and Tian (2013). (For interpretation of the references to colour in this figure legend, the reader is referred to the web version of this article.)

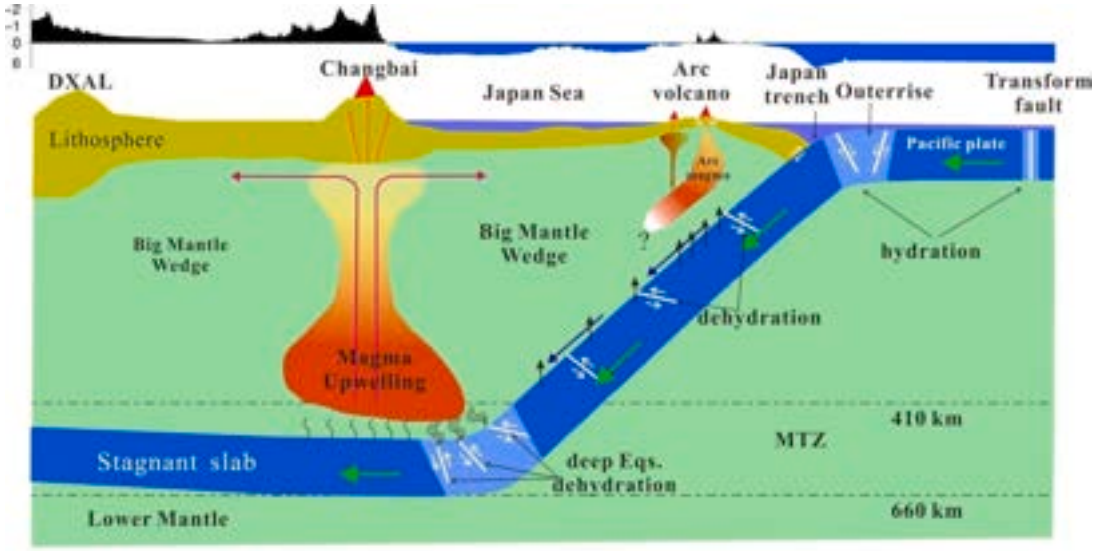

Fig. 12. A cartoon showing main features of the upper-mantle structure and dynamics in NE Asia, emphasizing the possible relationship between the Changbai intraplate volcanism and deep earthquakes in the Pacific slab (see text for details). DXAL, Daxing-Anling. After Zhao and Tian (2013).

Mesozoic, which was triggered by the Paleo-Pacific Plate subduction and subsequently led to the persistence of the stagnant slab and the BMW (Fig. 17a).

Regional seismograms of five earthquakes (60–300 km depths) were modeled to investigate both Vp and Vs structures of the NW Pacific subduction zone (Han et al., 2021). Both the Vp and Vs models show a low-V layer with a thickness of ~55–80 km lying above the 410-km discontinuity, extending laterally ~900 km from the Japan Sea to the NE Asian continental margin (Fig. 17b). With the dihedral angle approaching to zero around 400 km depth, a minute amount of melt atop the 410 km discontinuity caused by the hydrous slab may completely wet olivine grain boundaries, resulting in a low-V layer. This 410 low-V layer is a low-viscosity zone that would partially decouple the upper mantle from the MTZ. Zhao et al. (2022) determined a 3-D electrical resistivity model of the crust and upper mantle beneath the Longgang and Changbai volcanoes in NE China and suggested that the

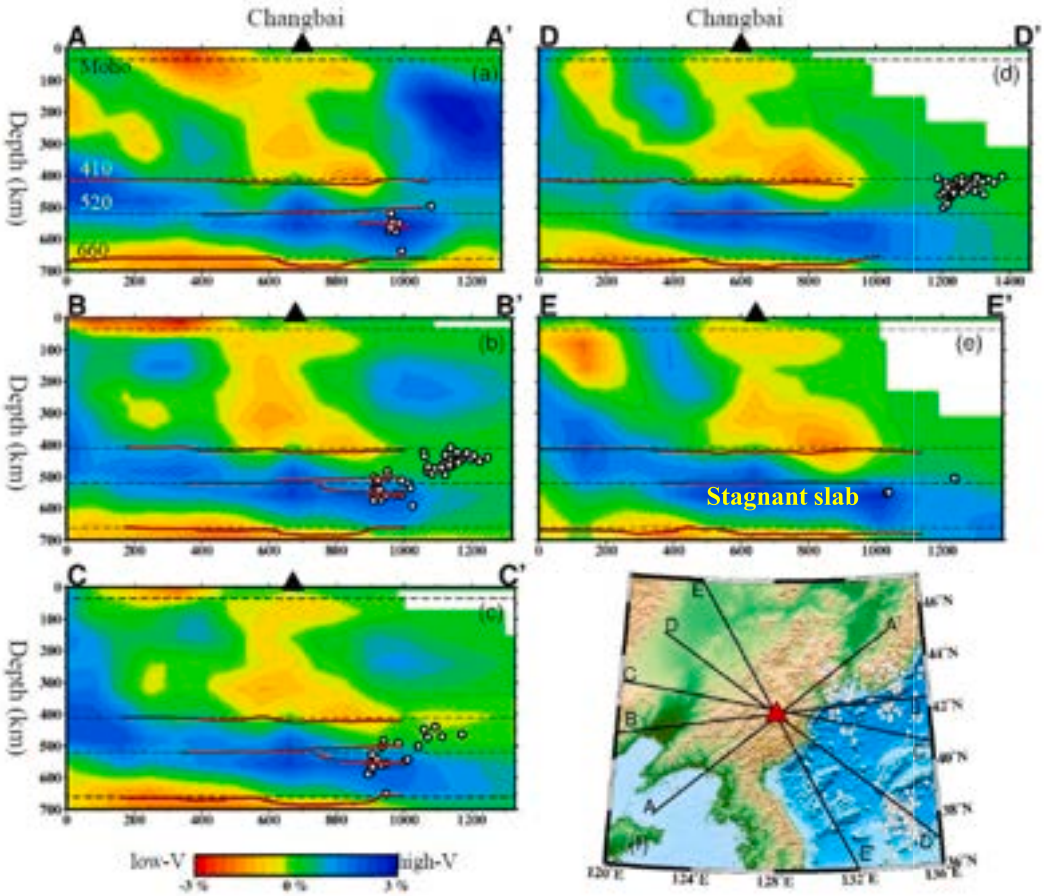

Fig. 13. Same as Fig. 10, but the red lines denote depth variations of the 410, 520 and 660 km discontinuities determined by teleseismic receiver functions (Tian et al., 2016). The white dots denote deep earthquakes with a 50 km width of each profile. (For interpretation of the references to colour in this figure legend, the reader is referred to the web version of this article.)

two intraplate volcanoes were caused by hot and wet upwelling flow in the BMW above the stagnant slab (Fig. 17c), supporting a previous resistivity result of the region (Ichiki et al., 2006).

Tang et al. (2023) investigated differences in the age, formation, spatial extent, and geodynamics between the eastern Asian BMW and the NE Asian BMW. They suggested that the eastern Asian BMW initially formed in the late Early Cretaceous and was active from 110 to 55 Ma due to rollback of the subducted Paleo-Pacific Plate and eastward deep mantle flow (Fig. 17d). This BMW affected the entire eastern Asian continental margin and controlled the late Mesozoic to early Paleogene tectonic evolution of the margin, including destruction of the North China Craton and reworking of the continental crust in South China. In contrast, the NE Asian BMW has been active from 20 Ma to the present due to rollback of the subducted Pacific Plate and eastward mantle flow, which has mainly affected NE Asia and resulted in different types of Cenozoic intraplate volcanism and the occurrence of deep earthquakes (Figs. 8 and 9).

In the past decade, anisotropic tomography has been actively conducted to map mantle flows in and around the BMW beneath East Asia (e.g., Fig. 7). The FVD of Vp azimuthal anisotropy in the mantle wedge beneath Japan is trench-normal, reflecting subduction-induced convection (e.g., Wang and Zhao, 2013; Wang and Zhao, 2021; Zhao et al., 2023a, 2023b). Beneath Kuril and Izu-Bonin where oblique subduction occurs, the FVD in the mantle wedge is nearly normal to the moving direction of the Pacific Plate, suggesting that the oblique subduction together with the complex slab morphology have disturbed the mantle flow (Liu et al., 2013; Wei et al., 2015; Niu et al., 2016). Similar features of mantle flow were also revealed by Vs anisotropic tomography down to ~300 km depth beneath the Japan Islands and the Japan Sea using Rayleigh-wave data (Liu and Zhao, 2016a). Depth variations of Vs azimuthal anisotropy in the BMW may reflect past Eurasian lithospheric deformation related to back-arc spreading during 21 to 15 Ma and complex present-day convection in the asthenosphere induced by subductions of both the Pacific and Philippine Sea plates.

Trench-parallel FVDs occur in the shallow portion of the subducting Pacific slab (< 80 km depth), whereas the deeper portion of the slab mainly exhibits trench-normal FVDs, except for the stagnant slab in the MTZ where NE-SW FVDs are evident (Ma et al., 2019). The FVDs in the subslab mantle change from a subduction-parallel trend at 80–400 km depths to a subduction-normal trend in the MTZ. Low-V anomalies were revealed beneath the Philippine Sea Plate where the FVD is NE-SW. The FVDs along the Izu-Bonin arc and in a slab gap exhibit a striking anticlockwise toroidal trend. All these features may reflect complex 3-D flows in the mantle wedge due to the slab tearing and dehydration processes.

Negative Vp radial anisotropy (i.e., $V_{horizontal} < V_{vertical}$) was revealed in the asthenosphere of the BMW under NE Asia, which may reflect mineral alignment caused by vertical flow in the BMW (Liang et al., 2022). Across the Tanlu fault zone in East China (e.g., Lei et al., 2020; Ji et al., 2025), the western and eastern parts of the BMW exhibit high and low Vp values, respectively (Fig. 18). Combining their tomographic results with surface geological features, Liang et al. (2022) suggested that the BMW convection includes upwelling flow beneath the Japan Sea and the Korean Peninsula, and downwelling flow beneath the Songliao and North China basins. The downwelling flow beneath the two basins is associated with diminishing volcanism and anomalous

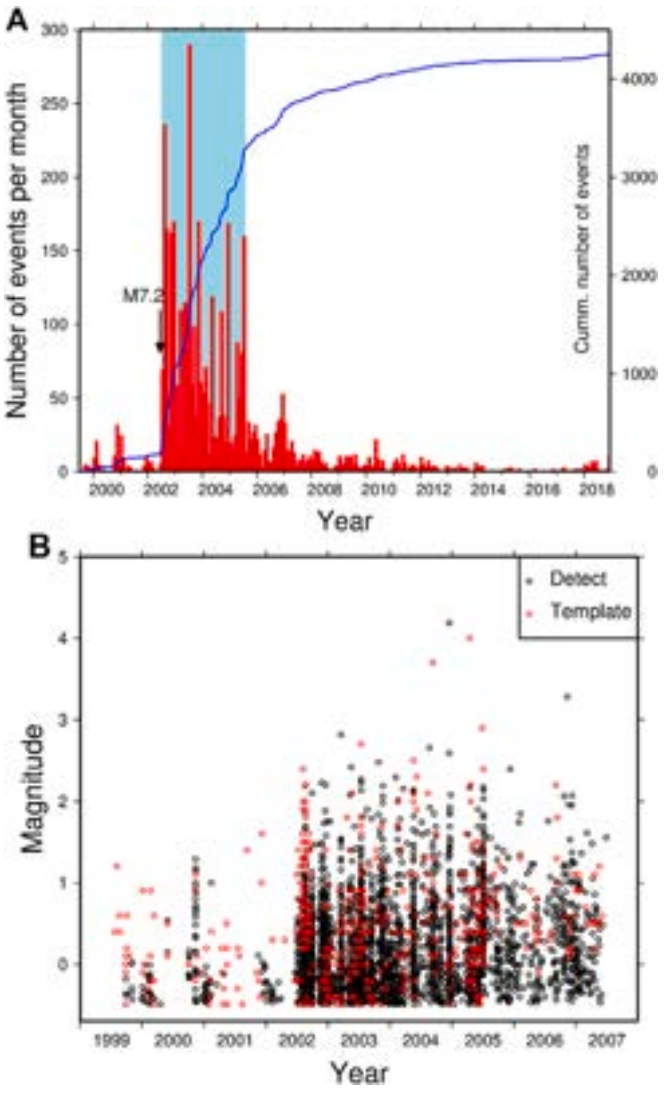

Fig. 14. (a) Monthly rates of local seismicity (red bars) from 1999 to 2018 in and around the Changbai volcano. The light blue shaded area indicates the time period of volcanic unrest. The blue curve represents the cumulative number of events. (b) Distribution of magnitudes versus time of the local events in and around the Changbai volcano. The red and black circles denote template events and detected events, respectively. After Liu et al. (2021). (For interpretation of the references to colour in this figure legend, the reader is referred to the web version of this article.)

tectonic subsidence since ~110 Ma. The great Tanlu fault zone in East China represents an important boundary for the BMW structure and dynamics (Fig. 18).

Recently, multiscale global tomography revealed whole-mantle 3-D Vp azimuthal anisotropy beneath NE Asia (Toyokuni et al., 2025). Even after anisotropy is considered, subslab hot mantle upwelling (SHMU) is clearly revealed beneath the subducted Pacific slab, indicating that SHMU is not a ghost artifact of isotropic tomography, as suggested by some previous studies (e.g., Confal et al., 2020). Beneath the Izu-Bonin region, the Vp anisotropic tomography clearly shows that the subducted slab is split into two blocks vertically in the lower mantle, indicating intermittent slab subductions (Zhao et al., 2017; Toyokuni et al., 2025).

5. Magmatic system of the Changbai volcano

In the past decade, many researchers have studied the detailed 3-D seismic velocity and electric resistivity structures of the crust and shallow mantle to understand magmatic plumbing systems of the CBV and other intraplate volcanoes in NE Asia. Some of the related results are shown in Figs. 19–23, which are briefly introduced here, from the crust to the upper mantle.

5.1. Seismic imaging

Detailed 3-D images of Vp, Vs and Vp/Vs ratio of the crust under the CBV were derived from local earthquake arrival times recorded at 360 portable seismographs deployed for one month in the CBV area (Yan et al., 2023). A high-Vp/Vs zone was revealed at ~5 km depth beneath the Tianchi caldera (Fig. 1b), accompanied with volcanic earthquakes, which may reflect a magma chamber (Fig. 19b). Intense seismicity within 2 km depth beneath the Tianchi caldera during 2002–2005 occurred directly above the magma chamber, which could be related to upward migration of high-pressure volatiles from the magma chamber. A mid-crustal magma chamber might provide continuous magmas feeding the shallow magma chamber and lead to ruptures of surrounding rocks, resulting in swarms of volcanic seismicity (Fig. 14). The diverse eruption styles of the CBV might be closely related to the multilevel structure of magma chambers in the upper and middle crust. Hammond et al. (2020) derived receiver functions using seismic records from both North Korea and NE China to study the CBV structure down to ~50 km depth. They revealed a thick crust (~40 km) and a high Vp/Vs ratio (up to 1.93) beneath the CBV. A significant velocity reduction was revealed at 4–8 km depths, dipping outward from the volcano, with shallowest depths centered beneath the CBV. This anomaly extends ~30 km from the volcano summit and possibly as far as neighboring volcanoes. The colocation of the velocity reduction with a zone of high-conductivity, low-V and low-density at the inflation source of the 2002–2005 CBV unrest indicates that partial melt is present directly beneath the CBV, likely recharged during the episode of unrest.

A joint inversion of teleseismic receiver functions and Rayleigh-wave group velocity dispersions from ambient noise was conducted to determine Vs tomography down to 60 km depth under the CBV (Zhu et al., 2019; Fig. 19a). The result shows a thick crust (~40 km) with a high Vp/Vs ratio (~1.8) beneath the CBV. A low-Vs body appears at 8–15 km depths directly beneath the volcano, extending ~100 km in the north–south direction, which may be a large mush zone or an assembly of many small magma batches. The Moho is depressed by 5–10 km and a low-Vs anomaly appears in the uppermost mantle beneath the CBV. These features may indicate an upwelling channel of the asthenospheric material with a high mafic composition, and the mafic intrusion attaches to the bottom of the crust and thus deepens the Moho beneath the volcano. Fan et al. (2022) determined a fine 3-D Vs model of CBV down to 60 km depth by applying waveform tomography to ambient noise recorded in both China and North Korea (Fig. 21f). They revealed a 3-D architecture of the CBV magma plumbing system, characterized by a prominent lower-crustal mush zone with an estimated melt fraction of ~1.5–3.6 %, which is sourced from upwelling asthenosphere through a narrow vertical conduit in the uppermost mantle.

To understand the CBV magmatic evolution, Kim et al. (2017) used ambient-noise tomography to image the lithospheric structure down to 120 km depth beneath the CBV and its surrounding areas (Fig. 19c). They made multiple measures of ambient noise dispersion with different methods, and conducted a joint inversion of the multiple datasets. Their results show a thick crust (~40 km) and a high-Vs anomaly at 20–40 km depths, which extends to ~100 km north from the CBV and is accompanied by a rapid Vs decrease beneath the mantle lid (~80 km depth). This structure was interpreted as a consequence of compositional partitioning caused by mafic underplating and overlying cooled felsic layers as a result of fractional crystalization. Tang et al. (2022) determined 3-D Vs tomography down to 120 km depth under NE China by jointly inverting receiver functions and fundamental-mode Rayleigh wave data (Fig. 20). Their result shows a nearly constant Vs of 3.4–3.6 km/s from

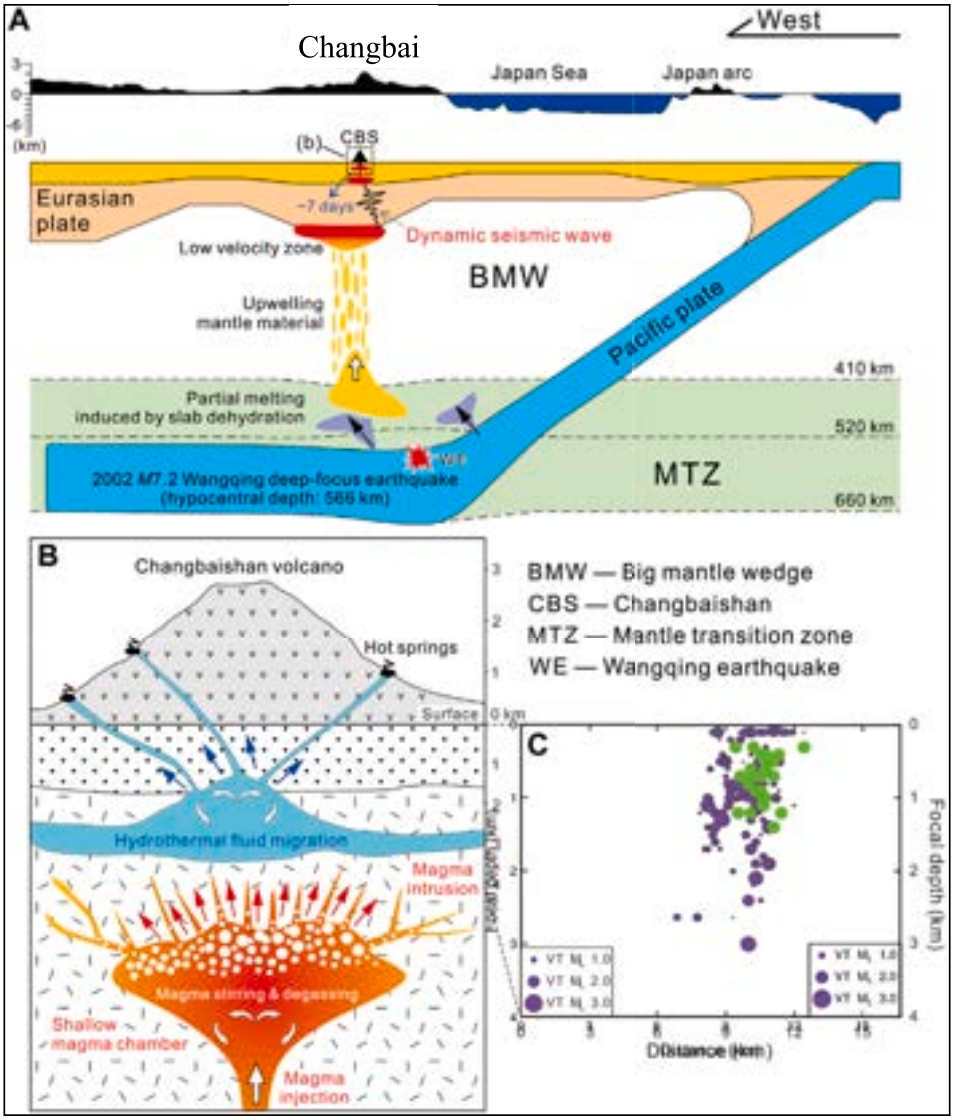

Fig. 15. (a) A conceptual model showing magma migration from a deep source to a shallow reservoir of the CBV in response to dynamic stress perturbations related to the 2002 M7.2 deep earthquake in the stagnant Pacific slab (see Fig. 8). An upwelling plume derived from the MTZ is shown as the magma origin of the CBV based on seismic tomography (Zhao et al., 2009) and basalt geochemistry (Zhang et al., 2018). The 410, 520, and 660 km discontinuities are from Tian et al. (2016) shown in Fig. 12 and Fig. 13. (b) Hypothetical magmatic and hydrothermal processes corresponding to the 2002–2005 unrest of the CBV. Injection of deep-sourced magmas into the shallow magma chamber led to anomalous magma stirring and degassing, which pressurized the shallow magma chamber and facilitated intrusion of gas-enriched magmas through cracks above the magma body. Hydrothermal fluid migration was influenced by crack intrusion of magmas. (c) A north-south vertical cross-section of local seismicity under the CBV. The green dots indicate harmonic spectra events. The purple dots indicate volcano-tectonic events with different magnitudes. After Liu et al. (2021). (For interpretation of the references to colour in this figure legend, the reader is referred to the web version of this article.)

shallow to deep crystalline crust, which was attributed to a high thermal gradient. Some high-Vs anomalies in the crust beneath the Songliao Basin (see Fig. 1c) may reflect solidified late-Mesozoic mafic intrusions. In the upper mantle, low-Vs zones appear below the CBV and the Lesser XingAn mountain range, suggesting asthenospheric mantle upwelling. Moderately low-Vs zones exist beneath the Halaha and Abaga volcanoes, reflecting pathways of magma ascent from the asthenosphere. The average depth of the lithosphere-asthenosphere boundary increases from ~70 km under CBV to ~100 km below the Songliao Basin, and reaches ~110–120 km beneath the Greater XingAn mountain range in the west.

Vs tomography down to 160 km depth beneath the CBV and its adjacent areas was determined by jointly inverting group and phase velocity dispersions from ambient noise and seismic surface waves (Li et al., 2023; Fig. 19d). A low-Vs zone exists in the crust beneath the CBV, indicating a hot magma chamber. The Longgang volcano is also characterized by a low-Vs anomaly, reflecting partial melt in the crust. In contrast, there is no notable low-Vs anomaly in the crust beneath the Jingpohu volcano (see Fig. 20c for its location). Low-Vs zones under the three volcanoes are interconnected in the upper mantle (Fig. 19d).

Teleseismic receiver functions were used to study the 3-D lithospheric structure down to 220 km depth beneath the CBV region (Zhang et al., 2024b; Fig. 21a-e). The results show a thick crust (~37 km) and a locally thin, weak lithosphere under the CBV, with its width of ~80 km at the Moho depth and ~ 200 km at the bottom of the lithosphere. These features suggest a trans-lithospheric magmatic system beneath the CBV, where hot material rises through the lithospheric mantle, underplates at the Moho depth, and forms magma chambers within the crust (Fig. 21e).

5.2. *Magnetotelluric soundings*

Li et al. (2020) investigated the 3-D electrical structure of the upper

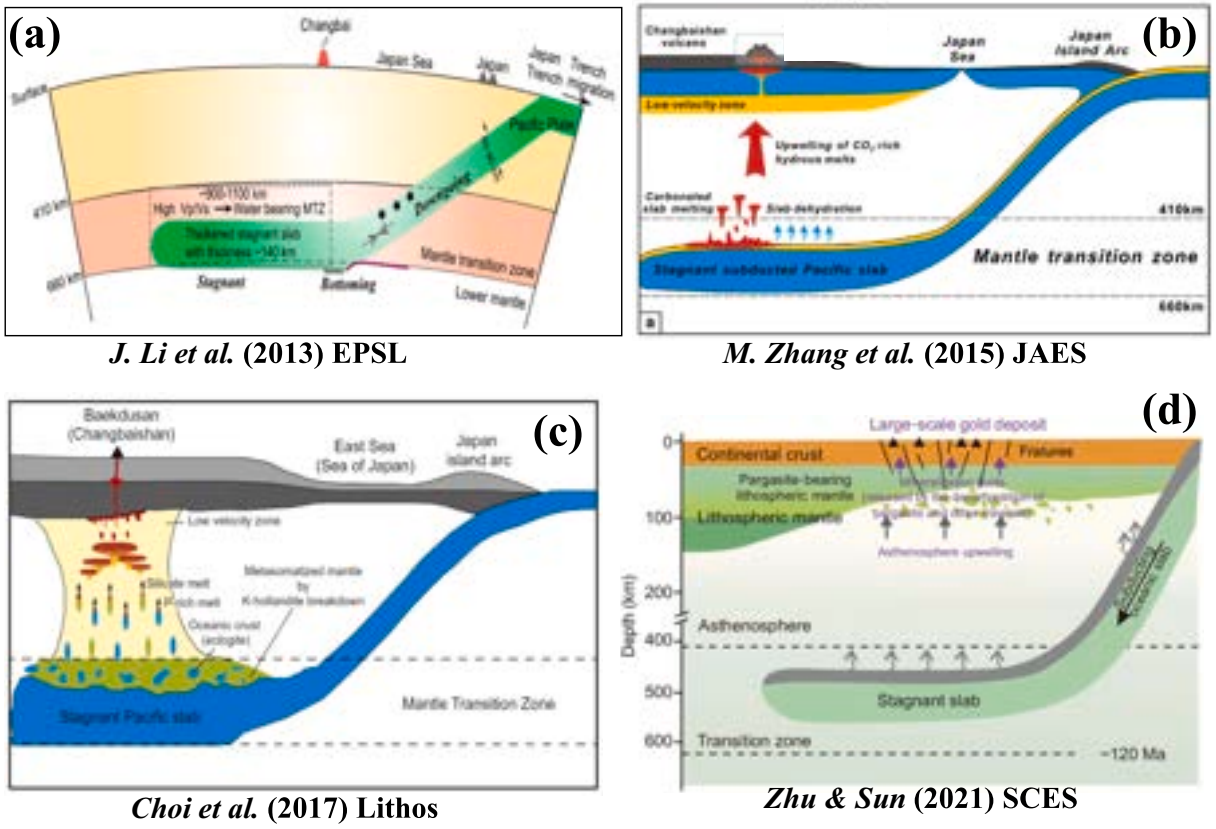

Fig. 16. Four models of the BMW beneath East Asia. The reference of each model is shown below each panel. See the text for details.

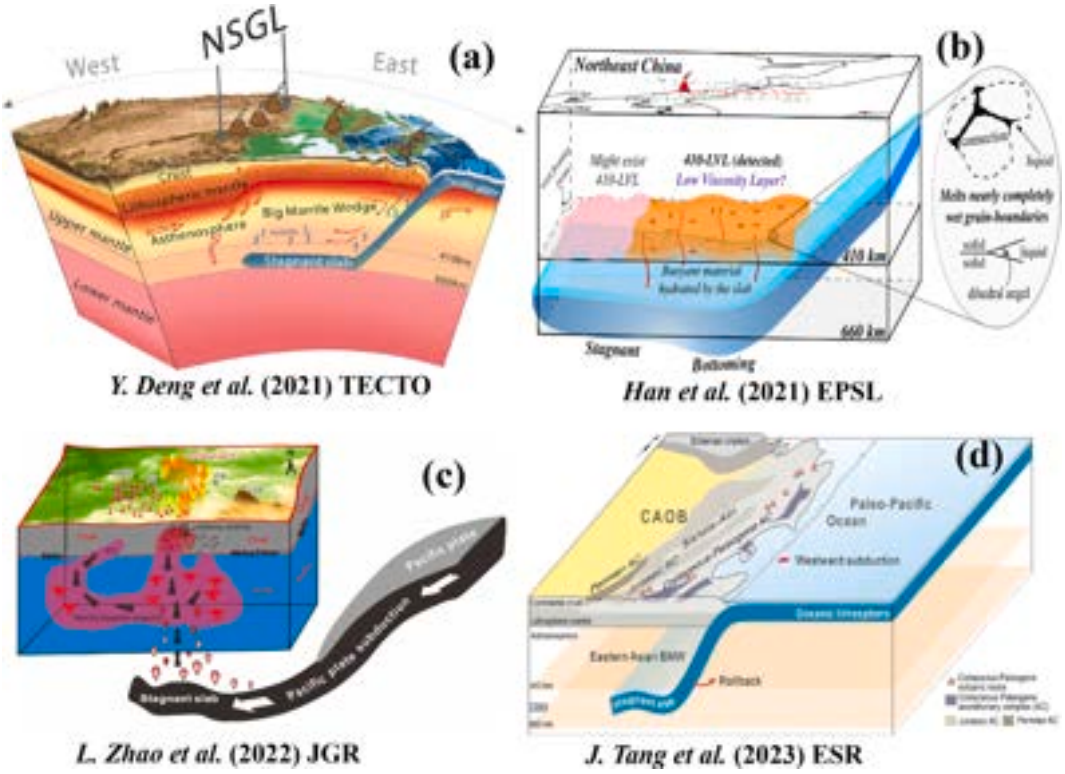

Fig. 17. Other four models of the BMW beneath East Asia. The reference of each model is shown below each panel. See the text for details.

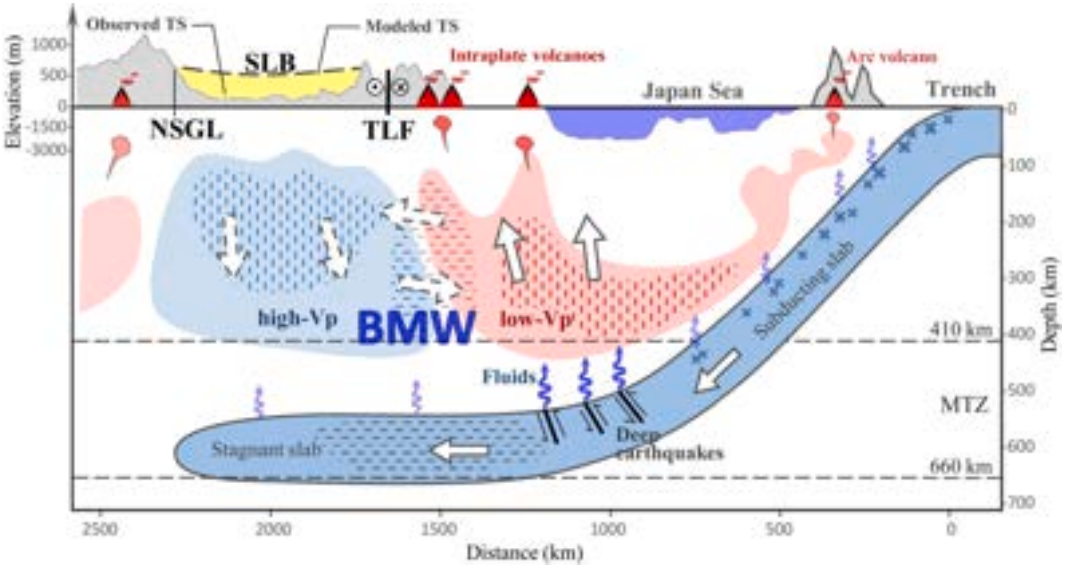

Fig. 18. A schematic diagram showing that downwelling asthenosphere in the western BMW triggers intraplate volcanism (red triangles) around the Songliao Basin (SLB) and anomalous tectonic subsidence (TS; yellow patch) of the SLB. Gray patches denote surface topography. Blue and red patches denote high and low Vp anomalies, respectively, in the BMW. White arrows denote mantle flow directions. Horizontal and vertical short bars denote positive and negative radial anisotropies, respectively. MTZ, mantle transition zone; NSGL, the North-South Gravity Lineament; TLF, the Tanlu fault zone. After Liang et al. (2022). (For interpretation of the references to colour in this figure legend, the reader is referred to the web version of this article.)

mantle beneath NE China (Fig. 22). They revealed multiple localized low-resistivity anomalies (LRAs) within the high-resistivity lithosphere, which partially coincide with the intraplate volcanoes on the surface. Three LRAs were revealed in the deep upper mantle beneath the Songliao Basin, whereas vein-like LRAs were found in the asthenosphere that connect the lithosphere and deep upper mantle. The LRAs were probably caused by fluid-induced melting. Li et al. (2020) and Xu et al. (2021) suggested that the 3-D electrical structure can be well interpreted by the BMW model (Zhao et al., 2004, 2009).

The Longgang volcano (LGV, see Fig. 22), located close to the CBV, is one of the largest intraplate monogenetic volcanoes in China, and its eruption lasted from the early Pleistocene to the Holocene. Zhao et al. (2022) determined a 3-D electrical resistivity model (Fig. 17c), which shows that the upper crust of the LGV and its surrounding areas hosts a high-resistivity body composed of volcanic rocks produced by massive eruptions during past volcanic episodes. As shown in Fig. 17c, two LRAs (C1 and C2) exist below 10 km depth under the LGV, and they merge in the lower crust and extend to the BMW, which were interpreted as magmatic channels. Magmas ascending along C1 probably caused an eruption ~1700 years ago. The zone C2 is larger and has lower resistivity than C1. The modern surface uplift and seismicity in the LGV are attributed to upwelling and intrusion along the C2 magmatic channel. An active fault passing through the LGV may also influence the upwelling of magma along C2, posing a hazard of future eruption. The LGV magmatic system may directly originate from the BMW (Fig. 17c), and the magma has experienced rapid ascent with limited crustal internal evolution (Zhao et al., 2022).

The LGV and CBV are considered to share a common magmatic source in the upper mantle (Fig. 22d). However, the two volcanoes have produced different types of eruptions. By inverting an magnetotelluric dataset that covered both volcanoes, Zhao et al. (2024b) obtained high-resolution electrical resistivity images (Fig. 23). Their results suggest that the two volcanoes have distinct magmatic plumbing systems, which may have caused their different eruptive styles. There is no magma chamber in the shallow crust beneath LGV (Fig. 23a), suggesting that rapid rise of magma from the mantle is responsible for producing a series of densely distributed volcanic cones in the LGV. This feature is consistent with the observation that abundant mantle xenoliths occur in relatively young volcanic materials at the LGV (e.g., Zhang et al., 2018; Zhang et al., 2024a). In contrast, a magma chamber exists in the upper crust beneath the CBV (Fig. 23a), where the fractional crystallization and mixing of magma has occurred. This magma chamber has facilitated multiple centralized eruptions, and thereby has led to the formation of the large CBV volcanic cone. These results indicate that different crustal structures may have caused the different eruptive activities of the LGV and CBV (Fig. 23c).

6. Discussion

6.1. Is there a slab hole under Changbai?

As mentioned above, there is a general consensus that the subducting Pacific slab is horizontally stagnant in the MTZ, forming a BMW system beneath NE Asia. As a result, the BMW has been widely invoked as the first-order geodynamic mechanism responsible for continental intraplate volcanism in East Asia, in terms of material contribution and dynamic mechanism (Zhao et al., 2004, 2009; Zhang et al., 2018). However, the existence of a hole in the stagnant Pacific slab beneath the CBV remains a subject of debate. From the perspective of subduction dynamics, the presence of a slab hole would cast uncertainties on chemical geodynamics of continental intraplate volcanism in NE Asia, especially for the CBV, which has been the main focus of this debate.

In the past decade, several seismological studies have been conducted using data recorded by a portable seismic network (NECESSArray) deployed in NE China during 2009–2011 (Fig. 20a). Tang et al. (2014) derived a tomographic model from teleseismic relative travel times recorded by the NECESSArray, revealing a low-V anomaly within the stagnant Pacific slab under the CBV. They interpreted this low-V anomaly as a slab hole in the MTZ and suggested that the CBV was produced by hot upwelling flow from the uppermost mantle through the slab hole. However, other tomographic models derived from absolute P and S travel times show higher velocities in the slab under the CBV, and so do not support the existence of a slab hole (Takeuchi et al., 2014; Wei et al., 2015; Chen et al., 2017; Ma et al., 2018; Lei et al., 2018; Liang et al., 2022).

Teleseismic tomography using relative travel-time data, originally proposed by Aki et al. (1977), is a popular and widely used tool for studying the upper mantle structure. However, this method has an

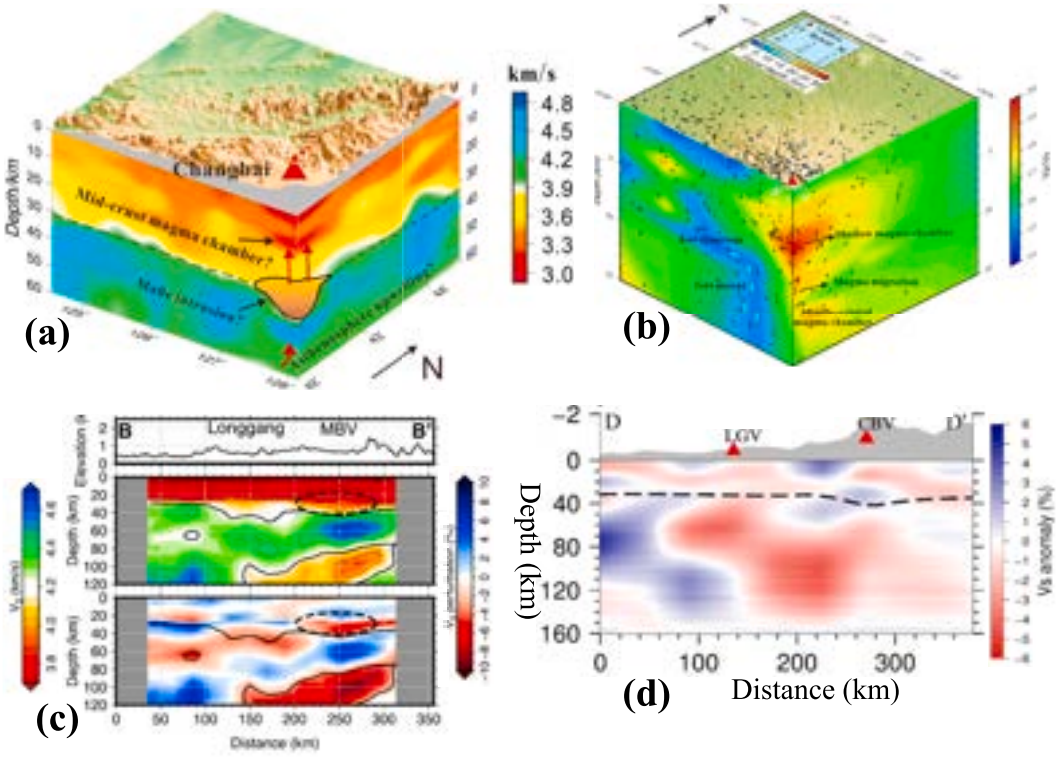

Fig. 19. (a) Vertical cross-sections of Vs tomography showing main features of the lithospheric structure beneath the CBV, emphasizing the possible relationship between crustal heterogeneities and mantle upwelling (Zhu et al., 2019). The dashed line denotes the Moho discontinuity from the receiver-function stacking. The red arrows indicate the ascent of magma beneath the CBV. (b) Vertical cross-sections of Vp/Vs image down to 15 km depth showing structures of a potential crustal magma chamber and the plumbing system of the CBV (Yan et al., 2023). The star and circle symbols denote volcanic-tectonic and hybrid events, respectively. Red and blue colors denote high and low Vp/Vs ratios, respectively, whose scale is shown on the right. (c) East-west vertical cross-section of Vs tomography passing through the Longgang and Changbai (MBV) volcanoes (Kim et al., 2017). The surface topography is shown at the top, Vs in the middle, and Vs perturbation to the mean Vs of each depth at the bottom. The Vs scale is shown on the left. The Vs perturbation scale is shown on the right. The anomalous structure beneath the MBV (CBV) is indicated by the dashed line. Thin dashed contours are presented with an interval of 0.2 km/s in the middle panel. Contour lines with Vs = 4.2 km/s are marked with solid lines in the middle and bottom panels to roughly indicate the Moho (~30–40 km depth) and the bottom of the lithosphere (> 60 km depth). (d) East-west vertical cross-section of Vs tomography passing through the Longgang (LGV) and Changbai (CBV) volcanoes (red triangles) determined by Li et al. (2023). The Vs perturbation scale is shown on the right. The surface topography is shown as gray patch at the top. The black dashed line denotes the Moho discontinuity. (For interpretation of the references to colour in this figure legend, the reader is referred to the web version of this article.)

inherent limitation, that is, the background mean velocity in the study volume is removed during the computation of relative travel times. Thus, teleseismic tomography alone is unable to recover the real shape of network-wide features at a given depth range beneath a local seismic network (e.g., Bastow, 2012), such as the wide and flat stagnant slab in the MTZ beneath NE Asia (Chen et al., 2017; Jia et al., 2022). This problem can be resolved by a simultaneous inversion of teleseismic relative travel-time residuals and absolute arrival-time data of local and regional earthquakes (e.g., Zhao et al., 2009; Chen et al., 2017), or by incorporating surface-wave data (e.g., Liu and Zhao, 2016b).

A recent study of double-difference tomography also suggested the existence of a slab hole under the CBV (Gao et al., 2025). However, updated whole-mantle tomography of NE Asia found no such feature under the CBV (Toyokuni et al., 2025). We examined the hypocentral parameters of the local and regional earthquakes and arrival-time data used by Gao et al. (2025) and found that, for many of their relocated events, the focal depths were < 0 km, suggesting large uncertainties in their hypocentral locations. Such poor hypocentral locations would undoubtedly affect the accuracy of their tomographic model.

Zhang et al. (2018) pointed out that the slab hole issue might not be resolved by seismological methods alone, and proposed to investigate this issue using multidisciplinary approaches. They considered the following two scenarios. The first is that entrained sub-slab asthenosphere (ESSA) ascends via a slab hole under the CBV, then the following inferences were made. (1) The ESSA layer is expected to be thin (10–30 km; Phipps Morgan et al., 2007; Long and Silver, 2009), so it is hard to feed the big slab hole (> 100 km wide and > 250 km high) as well as the plume at depths of 410 to ~100 km (the bottom of lithosphere). (2) Previous tomographic studies have shown that the detected sub-slab low-V anomaly under NE Asia is limited to ~410 km depth (Obayashi et al., 2006; Honda et al., 2007). Thus, the ESSA is unlikely to descend deeper due to barriers at the 410 and 660 km discontinuities. (3) Under the Japan-Kuril trench, shear-wave splitting measurements (Lynner and Long, 2014) and P-wave anisotropic tomography (Wei et al., 2015; Ma et al., 2019; Toyokuni et al., 2025) have shown trench-parallel sub-slab fast anisotropy, reflecting trench-parallel sub-slab flow field due to trench migration (Russo and Silver, 1994; Long, 2013), rather than downward slab-entrained flows. (4) There might be a gap between the Izanagi slab and the Pacific slab (i.e., the Izanagi-Pacific ridge), which formed at ~60–50 Ma (Seton et al., 2015), long before the onset of Changbai volcanism (~5 Ma).

The second scenario is that the source of sub-slab materials is the lower mantle. Beneath the CBV, however, all tomographic models to date show no evidence of a mantle plume rising from the CMB (e.g., Zhao, 2004; Tang et al., 2014; Toyokuni et al., 2025). Even if there is counterflow in response to the Izanagi slab sinking to the lower mantle, this does not necessitate a slab hole in the stagnant Pacific slab. Zhang et al. (2018) also mentioned two lines of geochemical evidence against the second scenario. One is excess mantle potential temperature of the CBV magma. To date, related geochemical results of the CBV magma (e.

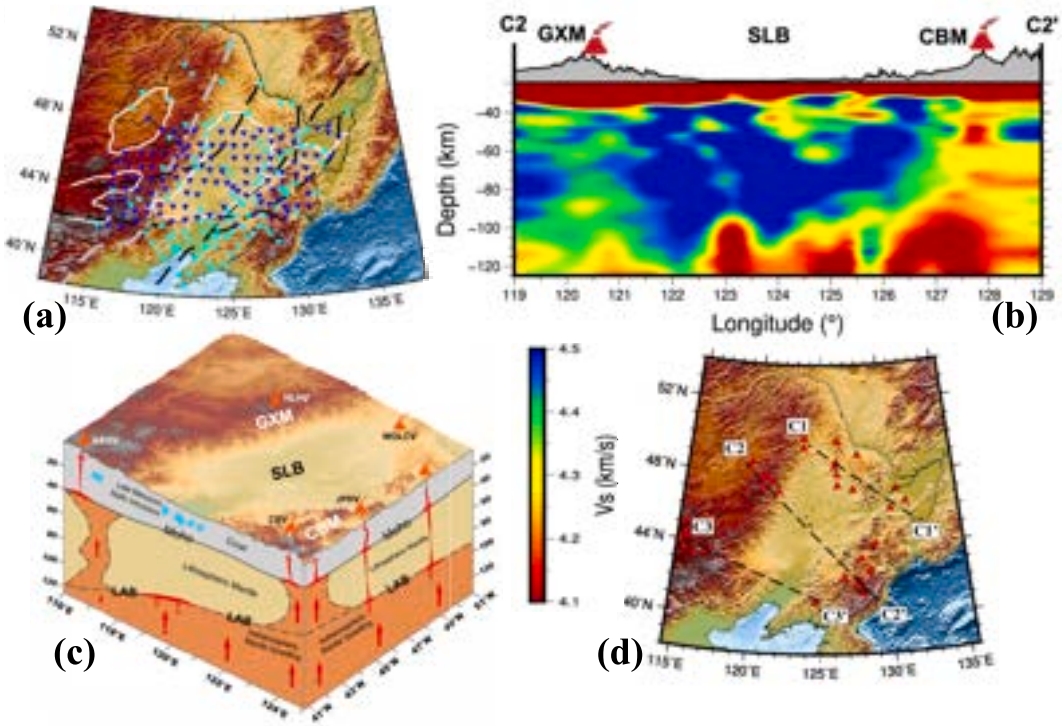

Fig. 20. (a) Topographic map of NE Asia. The gray dashed line denotes the North South Gravity Lineament (NSGL). White lines outline the main sedimentary basins. The cyan inverted triangles denote 107 permanent network stations. The blue inverted triangles denote 118 NECESSArray portable stations. (b) Vertical cross-section of Vs tomography along profile C2-C2' as shown in (d). The Vs scale is shown beside (c). CBM, Changbai mountain; GXM, Greater Xing'an mountain range; SLB, Songliao Basin. (c) A 3-D cartoon showing the main structural features beneath NE China, including the lithospheric thickening westward, and the Cenozoic volcanic/magmatic mechanism at lithospheric and sublithospheric levels. CBV, Changbai volcano; JPHV, Jingpohu volcano; WDLCV, Wudalianchi volcano; HLHV, Halaha volcano; ABGV, Abaga volcano; LAB, Lithosphere-Asthenosphere Boundary. (d) The red triangles denote active intraplate volcanoes in NE Asia. After Tang et al. (2022). (For interpretation of the references to colour in this figure legend, the reader is referred to the web version of this article.)

g., Kuritani et al., 2019) do not prove the magma source to be from the lower mantle. The other geochemical evidence is the helium isotope data, which do not support either the presence of lower mantle materials in the magma source of the CBV (e.g., Zhang et al., 2015).

Therefore, the slab hole model is not preferred for explaining the CBV magmatism. Even if sub-slab materials are involved via a slab hole, their contribution to CBV magma generation is likely negligible (Zhang et al., 2018). To resolve this issue definitively, much higher-resolution Vp and Vs tomography is required. For this purpose, it is necessary to install a dense seismograph network in North Korea and deploy many ocean-bottom seismometers in the Japan Sea. Hence, international cooperation among seismologists in the related countries (China, North Korea, South Korea, Japan, and Russia) will be very necessary and important.

6.2. *BMW in other regions*

In addition to East Asia, the BMW structure has been also found in several other regions. Beneath eastern Tibet, prominent low-V anomalies were revealed in the upper mantle, whereas a broad high-V zone was imaged in the MTZ (Lei et al., 2019). In addition, receiver-function imaging revealed a thicker MTZ in the area. Hence, Lei et al. (2019) suggested that a BMW exists under eastern Tibet, which could explain the origin of the active Tengchong volcano and the generation of large crustal earthquakes in the region. The Tengchong volcano is attributed to hot and wet upwelling flow in the BMW and fluids from dehydration reactions of the subducted Indian slab in the MTZ. The 2008 Wenchuan earthquake (M8.0) took place in a transitional belt from the low-V Songpan-Ganzi block to the high-V Sichuan Basin, and its occurrence was affected by the BMW structure and associated process (Lei et al., 2019).

Using global mantle tomography, Zhao et al. (2010) showed that the subducting Pacific slab becomes stagnant in the MTZ under western Alaska and the Bering Sea where many intraplate volcanoes exist. Clear low-V zones were revealed in the upper mantle above the stagnant slab, suggesting that the formation of those intraplate volcanoes was related to BMW processes and deep slab dehydration as well. This proposal has been confirmed by recent Vp anisotropic tomography (Liang et al., 2024). Corner flow in the mantle wedge above the subducting Pacific slab and toroidal flow in the BMW were revealed, which may have caused the Cenozoic intraplate volcanoes in western Alaska and the Bering Sea. The BMW above the subducted Farallon/Nazca slab might also cause Cenozoic intraplate magmatism in Patagonia (Navarrete et al., 2020).

Toyokuni and Zhao (2023) determined detailed 3-D Vp tomography of the whole mantle beneath the northern hemisphere (north of ~30°N latitude). Their results clearly show the subducted Izanagi and Farallon slabs penetrating into the lower mantle beneath Eurasia and North America, respectively. In the region from Canada to Greenland, a stagnant slab lying below the 660 km discontinuity was revealed. Because this slab has a texture indicative of subducted oceanic ridges, the slab might be composed of the Farallon and Kula slabs that had subducted during ~60–50 Ma. During that period, a complex rift system represented by the division between Canada and Greenland was developed. The oceanic ridge subduction and hot upwelling in the BMW caused a tensional stress field, which might have induced these complex tectonic events.

The Vrancea region of Romania exhibits a unique pattern of seismic activity, characterized by nearly vertical distributions of intermediate-depth earthquakes at depths of 60–180 km. These events appear to occur within the subducting Vrancea slab. Toyokuni and Zhao (2025) conducted a 3-D Vp tomography of the whole mantle beneath the

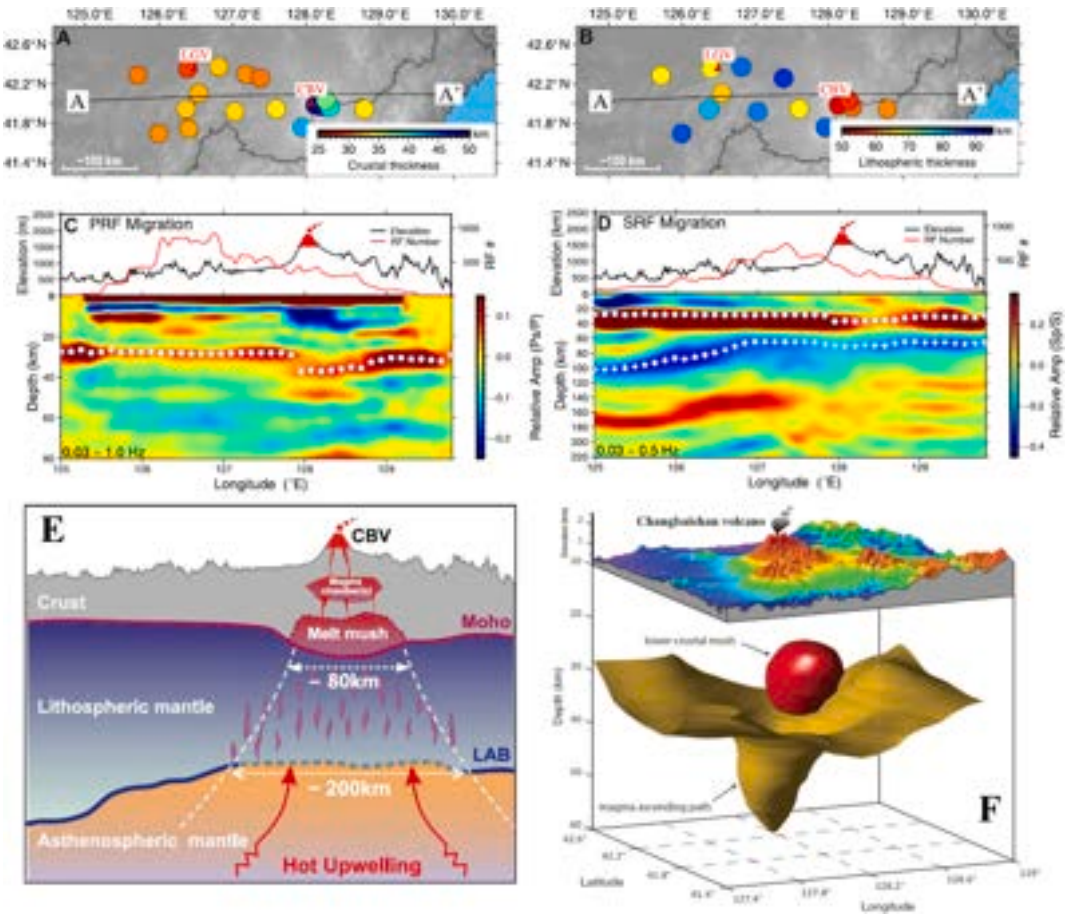

Fig. 21. (a-e) Teleseismic receiver function (RF) imaging of the lithospheric structure beneath the Changbai (CBV) and Longgang (LGV) volcanoes (Zhang et al., 2024b). (a) Crustal and (b) lithospheric thicknesses from slowness stack and time-depth conversion. Poststack depth-migrated images of (c) Ps receiver function (PRF) and (d) Sp receiver function (SRF) along profile A-A′. Pms phases are marked by white dots, and negative SLp phases are marked by white crosses. (e) A cartoon of trans-lithospheric magmatic system beneath the CBV. Hot upwelling asthenospheric material penetrates lithospheric mantle, underplates at the Moho, and forms magma chambers at the shallow depths. LAB, lithosphere-asthenosphere boundary. (f) A 3-D view of the magma plumbing system down to 60 km depth beneath the CBV (Fan et al., 2022). The red ellipsoid-like body, which is enclosed by an isosurface of Vs = 3.45 km/s, is interpreted as the lower-crustal mush zone, whereas the yellowish curved surface represented by an isosurface of Vs = 3.80 km/s indicates the magma ascending path in the uppermost mantle. (For interpretation of the references to colour in this figure legend, the reader is referred to the web version of this article.)

eastern Mediterranean region. Their results show that the subducting Vrancea slab is surrounded by hot mantle upwelling in the BMW associated with the descent of the African/Tethys slab into the MTZ. This dynamic environment may have enhanced slab dehydration, thereby generating the observed seismicity in the Vrancea region.

Global tomographic studies have shown that, as subducting slabs reach the MTZ, some tend to flatten and stagnate, whereas others descend into the lower mantle (e.g., Fukao et al., 2001; Zhao, 2004, 2015). This variable resistance to slab sinking can influence long-term thermal and chemical mantle circulation. Goes et al. (2017) reviewed observational constraints and geodynamic models and pointed out that neither the increase in viscosity between upper and lower mantle (likely by a factor of 20–50) nor the coincident endothermic phase transition in the main mantle silicates (with a likely Clapeyron slope of −1 to −2 MPa/K) suffice to stagnate slabs. However, the two factors together provide enough resistance to temporarily stagnate subducting slabs, if they subduct accompanied by significant trench retreat. An older, stronger plate is easier to induce trench retreat, so back-arc spreading and flat slab subduction tend to occur in old subduction zones, such as western Pacific and East Asia. Slab viscosities that are ~2 orders of magnitude higher than the surrounding mantle (effective yield stresses of 100–300 MPa) lead to similar styles of deformation as those revealed by seismic tomography and slab earthquakes. The current stagnant Pacific slab beneath NE Asia seems to have remained in the MTZ for less than 20 m.y. (e.g., Liu et al., 2017). Since modeled slab destabilization takes more than 100 m.y., lower-mantle entry is apparently usually triggered (e.g., by changes in plate buoyancy). Complex shapes of slabs in the lower mantle are caused by sinking and subsequent deformation of originally stagnated slabs, which can retain flat geometries in the uppermost lower mantle, fold as they sink deeper, and eventually form bulky shapes in the deep mantle (Goes et al., 2017).

Therefore, the BMW is a widespread and significant structure beneath modern convergent plate margins as revealed by seismic tomography, yet it is rarely identified in fossil convergent systems. Recently, a BMW was suggested to exist beneath the Western Mongolia Collage during the early to middle Paleozoic based on a comprehensive chronology of geological events that characterized the accretionary orogen in that region (Cui et al., 2024). The trench-arc system initially developed above a NE-dipping subduction zone, with subduction-related arc magmatism clustered at ~530–490 Ma. The westward migration of the arc was likely driven by slab rollback and trench retreat, leading to gradual formation of a BMW as the slab stagnated in the MTZ. The BMW influenced the tectonic evolution of the entire Western Mongolia Collage, inducing Ordovician–Silurian intraplate magmatism in regions inboard of the migrating magmatic arc and the potential opening of the Mongol-Okhotsk Ocean. Westward movement of the trench-arc continued until the Devonian, resulting in back-arc basin formation in the Chinese Altai and intraplate magmatism in the Hovd

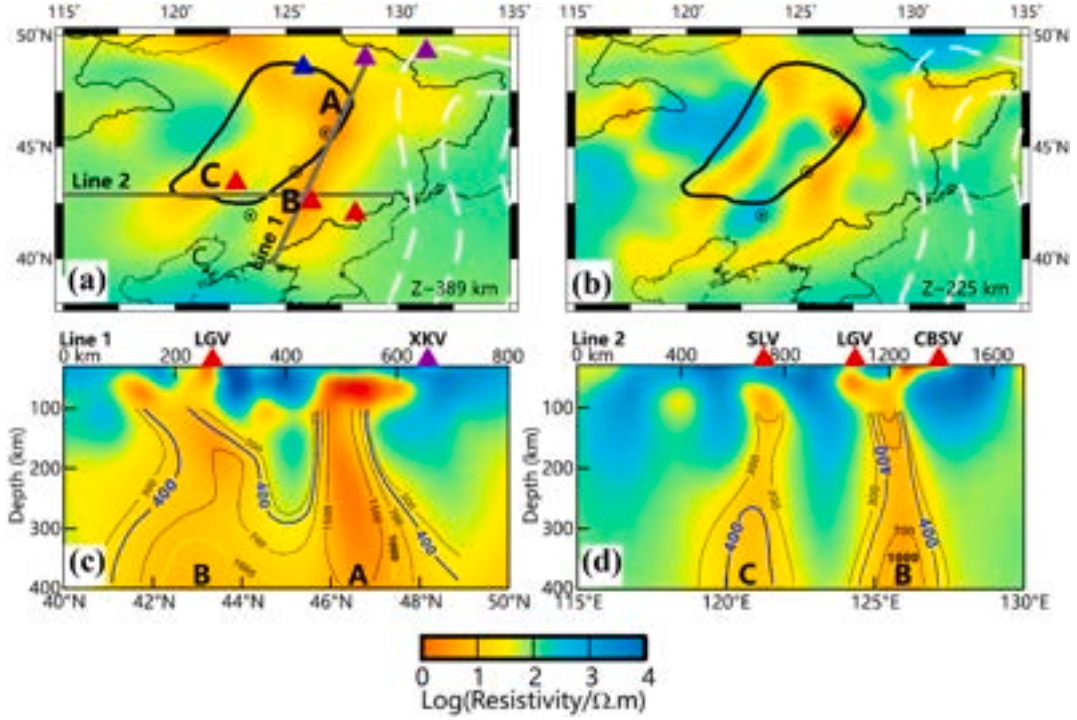

Fig. 22. (a, b) Map views of a 3-D resistivity model of NE China at 389 km and 225 km depths. A, B, and C indicate three sites where resistivity is <20 Ω·m. The black contour shows the range of the Songliao Basin. Circles denote locations of three provincial capitals in NE China (north to south: Harbin, Changchun, and Shenyang). White dashed lines represent depths to the subducting Pacific slab. Blue triangle: potassic basalt; purple triangles: high-Mg andesites; red triangles: sodic basalts. (c, d) Vertical cross-sections of the 3-D resistivity model along Lines 1 and 2 as shown in (a). Contours labeled 300, 400, 700, and 1000 denote inferred water content (in ppm). CBSV, Changbai volcano; LGV, Longgang volcano; SLV, Shuangliao volcano; XKV, Xunke volcano. Modified from Li et al. (2020) and Xu et al. (2021). (For interpretation of the references to colour in this figure legend, the reader is referred to the web version of this article.)

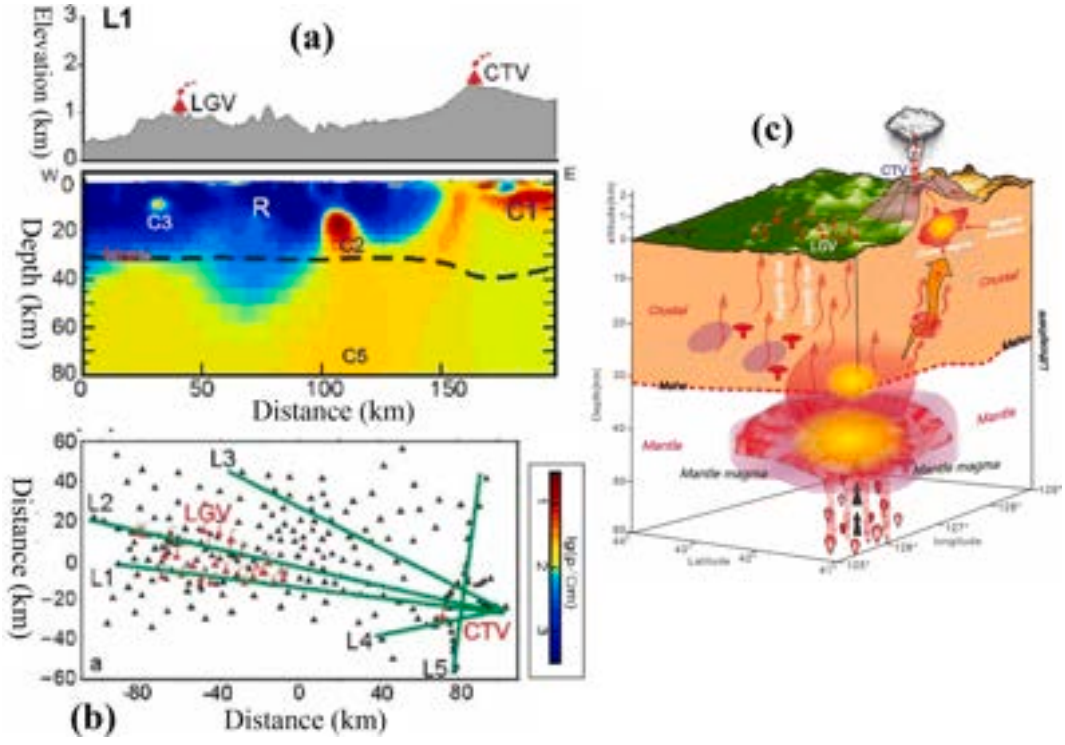

Fig. 23. (a) Vertical cross-section of a 3-D electrical resistivity model along the profile L1 as shown on map (b) where the triangles denote observation sites. The resistivity scale is shown beside (b). CTV, the Changbai-Tianchi volcano. LGV, the Longgang volcano. (c) A conceptual model summarizing eruption mechanisms of LGV and CTV. After Zhao et al. (2024b).

and Lake Zones of the Western Mongolia Collage, forming a trench–arc–back-arc and intraplate tectonic system. Mantle flows in the BMW could have impacted magmatism, basin migration, and the stress and thermal state of the overriding plate (Cui et al., 2024).

7. Conclusions

(1) The origin of the Changbai intraplate volcano (CBV) is hot and wet upwelling flow in the big mantle wedge (BMW) above the flat Pacific slab in the lower part of the mantle transition zone under East Asia.
(2) Fluids released from the Pacific slab by deep earthquake faulting provide additional magmas to feed the CBV, making it the largest and most active intraplate volcano in East Asia.
(3) Magma chambers are revealed in the crust and uppermost mantle under the CBV. This volcano has the potential to erupt again in the (near) future, so its activity should be closely monitored to mitigate potential hazards.
(4) International cooperation is necessary for better studies of the CBV, particularly through the deployment of seismic stations in North Korea and the Japan Sea.

CRediT authorship contribution statement

Dapeng Zhao: Writing – review & editing, Writing – original draft, Visualization, Validation, Supervision, Investigation, Formal analysis, Conceptualization. **Genti Toyokuni:** Writing – review & editing, Validation, Investigation. **YoungHee Kim:** Writing – review & editing, Validation, Investigation.

Declaration of competing interest

The authors declare that they have no known competing financial interests or personal relationships that could have appeared to influence the work reported in this paper.

Acknowledgements

This work was partially supported by Grant-in-aid for Scientific Research (No. 19H01996, 22K03749 and 23K22582) from Japan Society for the Promotion of Science, and the Earthquake and Volcano Hazard Reduction Research project of the MEXT, Japan. We are deeply grateful for the effective collaborations and helpful discussions with many colleagues and collaborators over the past decade, whose coauthored papers with us are included in the following list of references. Two anonymous referees provided thoughtful review comments and suggestions, which have improved this paper.

Data availability

No data was used for the research described in the article.

References

Aki, K., Christofferson, A., Husebye, E., 1977. Determination of the three-dimensional seismic structure of the lithosphere. J. Geophys. Res. 82, 277–296.
Asamori, K., Zhao, D., 2015. Teleseismic shear wave tomography of the Japan subduction zone. Geophys. J. Int. 203, 1752–1772.
Bastow, I., 2012. Relative arrival-time upper-mantle tomography and the elusive background mean. Geophys. J. Int. 190, 1271–1278.
Chen, C., Zhao, D., Tian, Y., Wu, S., Hasegawa, A., Lei, J., Park, J., Kang, I., 2017. Mantle transition zone, stagnant slab and intraplate volcanism in Northeast Asia. Geophys. J. Int. 209, 68–85.
Chen, Q., Wang, X., Jiang, J., Li, T., 2021. The Northwest Pacific subduction zone and its deep earthquake activity. Chin. J. Geophys. 64, 4394–4405.
Choi, H., Choi, S., Schiano, P., Cho, M., 2017. Geochemistry of olivine-hosted melt inclusions in the Baekdusan (Changbaishan) basalts: implications for recycling of oceanic crustal materials into the mantle source. Lithos 284, 194–206.
Confal, J., Bezada, M., Eken, T., Faccenda, M., Saygin, E., Taymaz, T., 2020. Influence of upper mantle anisotropy on isotropic P-wave tomography images obtained in the eastern Mediterranean region. J. Geophys. Res. Solid Earth 125 e2019JB018559.
Cui, X., Cawood, P., Sun, M., Zhao, G., 2024. Recognizing big mantle wedges in deep time: constraints from the Western Mongolia collage in Central Asia. Geology 52, 341–346.
Dasgupta, R., Lee, C., 2025. Deciphering the underlying hydrous plume geometry and dynamic topography of intraplate volcanoes: a computational fluid dynamic model analysis. Phys. Fluids 37, 046619.
Deng, Y., Xu, Y., Chen, Y., 2021. Formation mechanism of the North–South Gravity Lineament in eastern China. Tectonophysics 818, 229074.
Dokht, R., Gu, Y., Sacchi, M., 2016. Waveform inversion of SS precursors: an investigation of the northwestern Pacific subduction zones and intraplate volcanoes in China. Gondwana Res. 40, 77–90.
Fan, J., Zhao, D., 2021. Subslab heterogeneity and giant megathrust earthquakes. Nat. Geosci. 14, 349–353.
Fan, X., Guo, Z., Zhao, Y., Chen, Q., 2022. Crust and uppermost mantle magma plumbing system beneath Changbaishan intraplate volcano, China/North Korea, revealed by ambient noise adjoint tomography. Geophys. Res. Lett. 49 e2022GL098308.
Foulger, G., 2010. Plates Vs Plumes: A Geological Controversy. Wiley-Blackwell, 328 pp.
Foulger, G., Natland, J., Presnall, D., Anderson, D., 2005. Plates, plumes and paradigms. Geol. Soc. Am. Spec. Pap. 388, 881 pp.
Fukao, Y., Widiyantoro, S., Obayashi, M., 2001. Stagnant slabs in the upper and lower mantle transition region. Rev. Geophys. 39, 291–323.
Gao, F., Tian, Y., Zhao, D., Li, H., Liu, C., 2024. Shear wave splitting and mantle dynamics of the southern great xing'an Orogenic Belt. Tectonophysics 880, 230336.
Gao, L., Zhang, H., Myhill, R., Gao, J., Leng, W., 2025. Local slab penetration into lower mantle controls deep-focus seismicity and Changbaishan volcanism in Northeast China. Nat. Commun. 16, 2782.
Goes, S., Agrusta, R., van Hunen, J., Garel, F., 2017. Subduction-transition zone interaction: A review. Geosphere 13, 1–21.
Gu, Y., Okeler, A., Schultz, R., 2012. Tracking slabs beneath northwestern Pacific subduction zones. Earth Planet. Sci. Lett. 331, 269–280.
Guo, H., Zhao, D., Ding, Z., 2024. Anisotropic tomography and mantle dynamics of the North China craton. Geophys. J. Int. 236, 1455–1470.
Hammond, J., Wu, J., Ri, K., Wei, W., Yu, J., Oppenheimer, C., 2020. Distribution of partial melt beneath Changbaishan /Paektu volcano, China /Democratic People's Republic of Korea. Geochem. Geophys. Geosyst. 21 e2019GC008461.
Han, G., Li, J., Guo, G., Mooney, W., Karato, S., Yuen, D., 2021. Pervasive low-velocity layer atop the 410-km discontinuity beneath the Northwest Pacific subduction zone: implications for rheology and geodynamics. Earth Planet. Sci. Lett. 555, 116642.
Hayes, G., Wald, D., Johnson, R., 2012. Slab 1.0: a three-dimensional model of global subduction zone geometries. J. Geophys. Res. Solid Earth 117, B01302.
He, L., 2014. Numerical modeling of convective erosion and peridotite-melt interaction in big mantle wedge: implications for the destruction of the North China craton. J. Geophys. Res. Solid Earth 119, 3662–3677.
He, L., 2017. Wet plume atop of the flattening slab: insight into intraplate volcanism in East Asia. Phys. Earth Planet. Inter. 269, 29–39.
Honda, S., Morishige, M., Orihashi, Y., 2007. Sinking hot anomaly trapped at the 410 km discontinuity near the Honshu subduction zone. Japan. Earth Planet. Sci. Lett. 261, 565–577.
Hu, H., Zhao, D., Lin, J., Pilia, S., 2023. A slab window beneath North Sumatra revealed by P-wave mantle tomography. J. Geophys. Res. Solid Earth 128 e2022JB025976.
Huang, J., Zhao, D., 2006. High-resolution mantle tomography of China and surrounding regions. J. Geophys. Res. Solid Earth 111, B09305.
Huang, Z., Zhao, D., Hasegawa, A., Umino, N., Park, J., Kang, I., 2013. Aseismic deep subduction of the Philippine Sea plate and slab window. J. Asian Earth Sci. 75, 82–94.
Ichiki, M., Baba, K., Obayashi, M., Utada, H., 2006. Water content and geotherm in the upper mantle above the stagnant slab: interpretation of electrical conductivity and seismic P-wave velocity models. Phys. Earth Planet. Inter. 155, 1–15.
Ji, G., Lei, J., Zhao, D., 2025. Anisotropic tomography and seismotectonics of the central Tanlu fault zone in East China. Geophys. J. Int. 241, 1413–1431.
Jia, R., Zhao, D., Wu, J., 2022. P-wave anisotropic tomography of NE China: insight into lithospheric deformation, mantle dynamics and intraplate volcanism. Geophys. J. Int. 229, 1372–1391.
Kameyama, M., Nishioka, R., 2012. Generation of ascending flows in the big mantle wedge (BMW) beneath Northeast Asia induced by retreat and stagnation of subducted slab. Geophys. Res. Lett. 39, L10309.
Kanamori, H., 1971. Great earthquakes at island arcs and the lithosphere. Tectonophysics 12, 187–198.
Kim, S., Tkalčić, H., Rhie, J., 2017. Seismic constraints on magma evolution beneath Mount Baekdu (Changbai) volcano from transdimensional Bayesian inversion of ambient noise data. J. Geophys. Res. Solid Earth 122, 5452–5473. https://doi.org/10.1002/2017JB014105.
Kubota, T., Hino, R., Inazu, D., Suzuki, S., 2019. Fault model of the 2012 doublet earthquake, near the up-dip end of the 2011 Tohoku-Oki earthquake, based on a near-field tsunami: implications for intraplate stress state. Prog Earth Planet Sci 6, 67.
Kuritani, T., Ohtani, E., Kimura, J., 2011. Intensive hydration of the mantle transition zone beneath China caused by ancient slab stagnation. Nat. Geosci. 4, 713–716.
Kuritani, T., Xia, Q., Kimura, J., Liu, J., Shimizu, K., Ushikubo, T., Zhao, D., Nakagawa, M., Yoshimura, S., 2019. Buoyant hydrous mantle plume from the mantle transition zone. Sci. Rep. 9, 6549.

Lay, T., Duputel, Z., Ye, L., Kanamori, H., 2013. The December 7, 2012 Japan trench intraplate doublet (mw 7.2, 7.1) and interactions between near-trench intraplate thrust and normal faulting. Phys. Earth Planet. Inter. 220, 73–78.
Lee, S., Rhie, J., Park, Y., Kim, K., 2014. Topography of the 410 and 660 km discontinuities beneath the Korean peninsula and southwestern Japan using teleseismic receiver functions. J. Geophys. Res. Solid Earth 119, 7245–7257.
Lei, J., Zhao, D., 2005. P-wave tomography and origin of the Changbai intraplate volcano in Northeast Asia. Tectonophysics 397, 281–295.
Lei, J., Zhao, D., Xu, Y., Fan, Q., 2018. Is there a gap in the stagnant Pacific slab in the mantle transition zone under the Changbaishan volcano? Acta Petrol. Sin. 34, 13–22.
Lei, J., Zhao, D., Xu, X., Xu, Y., Du, M., 2019. Is there a big mantle wedge under eastern Tibet? Phys. Earth Planet. Inter. 292, 100–113.
Lei, J., Zhao, D., Xu, X., Du, M., Mi, Q., Lu, M., 2020. P-wave upper-mantle tomography of the Tanlu fault zone in eastern China. Phys. Earth Planet. Inter. 299, 106402.
Li, X., Yuan, X., 2003. Receiver functions in northeast China: implications for slab penetration into the lower mantle in northwest Pacific subduction zone. Earth Planet. Sci. Lett. 216, 679–691.
Li, J., Wang, X., Wang, X., Yuen, D., 2013. P and SH velocity structure in the upper mantle beneath Northeast China: evidence for a stagnant slab in hydrous mantle transition zone. Earth Planet. Sci. Lett. 367, 71–81.
Li, S., Weng, A., Li, J., Shan, X., Han, J., Tang, Y., Zhang, Y., Wang, X., 2020. Deep origin of Cenozoic volcanoes in Northeast China revealed by 3-D electrical structure. Sci. China Earth Sci. 63, 533–547. https://doi.org/10.1007/s11430-018-9537-2.
Li, H., Tian, Y., Zhao, D., Kumar, R., Li, H., Yan, D., Liu, C., 2023. Shear-wave tomography of the Changbai volcanic area in NE China derived from ambient noise and seismic surface waves. J. Asian Earth Sci. 258, 105482.
Liang, X., Zhao, D., Xu, Y., Hua, Y., 2022. Anisotropic tomography and dynamics of the big mantle wedge. Geophys. Res. Lett. 49 e2021GL097550.
Liang, X., Zhao, D., Hua, Y., Xu, Y., 2024. Big mantle wedge and intraplate volcanism in Alaska: insight from anisotropic tomography. J. Geophys. Res. Solid Earth 129 e2023JB027617.
Liu, J., 1999. Volcanoes in China. Science Press, Beijing, 219 pp.
Liu, R., 2000. Active Volcanoes in China. Seismological Press, Beijing, 114 pp.
Liu, X., Zhao, D., 2016a. Backarc spreading and mantle wedge flow beneath the Japan Sea: insight from Rayleigh-wave anisotropic tomography. Geophys. J. Int. 207, 357–373.
Liu, X., Zhao, D., 2016b. P and S wave tomography of Japan subduction zone from joint inversions of local and teleseismic travel times and surface-wave data. Phys. Earth Planet. Inter. 252, 1–22.
Liu, X., Zhao, D., Li, S., 2013. Seismic heterogeneity and anisotropy of the southern Kuril arc: insight into megathrust earthquakes. Geophys. J. Int. 194, 1069–1090.
Liu, X., Zhao, D., Li, S., Wei, W., 2017. Age of the subducting Pacific slab beneath East Asia and its geodynamic implications. Earth Planet. Sci. Lett. 464, 166–174.
Liu, G., Li, C., Peng, Z., Liu, Y., Zhang, Y., Liu, D., Zhang, M., Pan, B., 2021. The 2002–2005 Changbaishan volcanic unrest triggered by the 2002 M7.2 Wangqing deep focus earthquake. Front. Earth Sci. 8, 599329.
Long, M., 2013. Constraints on subduction geodynamics from seismic anisotropy. Rev. Geophys. 51, 76–112.
Long, M., Silver, P., 2009. Mantle flow in subduction systems: the subslab flow field and implications for mantle dynamics. J. Geophys. Res. Solid Earth 114, B10312.
Lu, M., Lei, J., Zhao, D., Ai, Y., Xu, X., Zhang, G., 2020. SKS splitting measurements in NE China: new insights into the Wudalianchi intraplate volcanism and mantle dynamics. J. Geophys. Res. Solid Earth 125 e2019JB018575.
Lynner, C., Long, M., 2014. Sub-slab anisotropy beneath the Sumatra and circum-Pacific subduction zones from source-side shear wave splitting observations. Geochem. Geophys. Geosyst. 15, 2262–2281.
Ma, X.Y., 1989. Lithospheric Dynamics Map of China and Adjacent Seas (1:4,000,000) and Explanatory Notes. Geological Publishing House, Beijing, China.
Ma, J., Tian, Y., Liu, C., Zhao, D., Feng, X., Zhu, H., 2018. P-wave tomography of Northeast Asia: constraints on the western Pacific plate subduction and mantle dynamics. Phys. Earth Planet. Inter. 274, 105–126.
Ma, J., Tian, Y., Zhao, D., Liu, C., Liu, T., 2019. Mantle dynamics of Western Pacific and East Asia: new insights from P-wave anisotropic tomography. Geochem. Geophys. Geosyst. 20, 3628–3658.
Maruyama, S., 1994. Plume tectonics. J. Geol. Soc. Jpn. 100, 24–49.
Navarrete, C., Gianni, G., Massaferro, G., Butler, K., 2020. The fate of the Farallon slab beneath Patagonia and its links to Cenozoic intraplate magmatism, marine transgressions and topographic uplift. Earth Sci. Rev. 210, 103379.
Niu, X., Zhao, D., Li, J., Ruan, A., 2016. P wave azimuthal and radial anisotropy of the Hokkaido subduction zone. J. Geophys. Res. Solid Earth 121, 2636–2660.
Obana, K., Fujie, G., Takahashi, T., Yamamoto, Y., Nakamura, Y., Kodaira, S., Takahashi, N., Kaneda, Y., Shinohara, M., 2012. Normal-faulting earthquakes beneath the outer slope of the Japan trench after the 2011 Tohoku earthquake: implications for the stress regime in the incoming Pacific plate. Geophys. Res. Lett. 39, L00G24.
Obayashi, M., Sugioka, H., Yoshimitsu, J., Fukao, Y., 2006. High temperature anomalies oceanward of subducting slabs at the 410 km discontinuity. Earth Planet. Sci. Lett. 243, 149–158.
Phipps Morgan, J., Hasenclever, J., Hort, M., Rupke, L., Parmentier, E., 2007. On subducting slab entrainment of buoyant asthenosphere. Terra Nova 19, 167–173.
Richard, G., Iwamori, H., 2010. Stagnant slab, wet plumes and Cenozoic volcanism in East Asia. Phys. Earth Planet. Inter. 183, 280–287.
Russo, R., Silver, P., 1994. Trench-parallel flow beneath the Nazca plate from seismic anisotropy. Science 263, 1105–1111.
Seton, M., Flament, N., Whittaker, J., Muller, R., Gurnis, M., Bower, D., 2015. Ridge subduction sparked reorganization of the Pacific plate-mantle system 60-50 million years ago. Geophys. Res. Lett. 42, 1732–1740.
Simkin, T., Siebert, L., 1994. Volcanoes of the World. Geoscience Press, Washington DC, 349 pp.
Simute, S., Steptoe, H., Cobden, L., Gokhberg, A., Fichtner, A., 2016. Full-waveform inversion of the Japanese Islands region. J. Geophys. Res. Solid Earth 121, 3722–3741. https://doi.org/10.1002/2016JB012802.
Tajima, F., Katayama, I., Nakagawa, T., 2009. Variable seismic structure near the 660 km discontinuity associated with stagnant slabs and geochemical implications. Phys. Earth Planet. Inter. 172, 183–198.
Takeuchi, N., Kawakatsu, H., Tanaka, S., 2014. Upper mantle tomography in the northwestern Pacific region using triplicated P waves. J. Geophys. Res. Solid Earth 119, 7667–7685.
Tang, J., Deng, Q., Zhao, G., 2001. Electric conductivity and magma chamber at the Tianchi volcano area in Changbaishan. Seismol. Geol. 23, 191–200.
Tang, Y., Obayashi, M., Niu, F., 2014. Changbaishan volcanism in Northeast China linked to subduction-induced mantle upwelling. Nat. Geosci. 7, 470–475.
Tang, Z., Julià, J., Mai, P., Mooney, W., Wu, Y., 2022. Shear-wave velocity structure beneath Northeast China from joint inversion of receiver functions and Rayleigh wave phase velocities: implications for intraplate volcanism. J. Geophys. Res. Solid Earth 127. https://doi.org/10.1029/2022JB023956 e2022JB023956.
Tang, J., Wang, F., Wang, Y., Long, X., Xu, W., 2023. Age, formation mechanisms, spatial extent, and geodynamic effects of the eastern and northeastern Asian big mantle wedges. Earth Sci. Rev. 237, 104324.
Tatsumi, Y., Maruyama, S., Nohda, S., 1990. Mechanism of backarc opening in the Japan Sea: role of asthenospheric injection. Tectonophysics 181, 299–306.
Tian, Y., Zhao, D., 2013. Reactivation and mantle dynamics of North China craton: insight from P-wave anisotropy tomography. Geophys. J. Int. 195, 1796–1810.
Tian, Y., Zhu, H., Zhao, D., Liu, C., Feng, X., Liu, T., Ma, J., 2016. Mantle transition zone structure beneath the Changbai volcano: insight into deep slab dehydration and hot upwelling near the 410-km discontinuity. J. Geophys. Res. Solid Earth 121, 5794–5808.
Toyokuni, G., Zhao, D., 2023. Ancient slabs beneath Arctic and surroundings: Izanagi, Farallon, and in-betweens. Prog Earth Planet Sci 10, 64.
Toyokuni, G., Zhao, D., 2024. Slab-plume interactions beneath Australia and New Zealand: new insight from whole-mantle tomography. Geochem. Geophys. Geosyst. 25 e2024GC011739.
Toyokuni, G., Zhao, D., 2025. Whole-mantle tomography beneath eastern Mediterranean and adjacent regions. Geophys. J. Int. 241, 1155–1172.
Toyokuni, G., Zhao, D., Kurata, K., 2022. Whole-mantle tomography of Southeast Asia: new insight into plumes and slabs. J. Geophys. Res. Solid Earth 127 e2022JB024298.
Toyokuni, G., Zhao, D., Takada, D., 2025. Whole-mantle isotropic and anisotropic tomography beneath Japan and adjacent regions. J. Geophys. Res. Solid Earth 130 e2024JB029593.
Turcotte, D., Schubert, G., 1982. Geodynamics. John Wiley and Sons Press, 450 pp.
Wang, J., Zhao, D., 2013. P-wave tomography for 3-D radial and azimuthal anisotropy of Tohoku and Kyushu subduction zones. Geophys. J. Int. 193, 1166–1181.
Wang, Z.W., Zhao, D., 2021. 3D anisotropic structure of the Japan subduction zone. Sci. Adv. 7, eabc9620.
Wang, J., Zhu, D., Zhang, Z., He, J., Chen, L., Zhao, D., Yao, Z., 2025. Seismic evidence for large-scale intraslab heterogeneity beneath Northeast Japan. J. Geophys. Res. Solid Earth 130 e2024JB030046.
Wei, W., Xu, J., Zhao, D., Shi, Y., 2012. East Asia mantle tomography: new insight into plate subduction and intraplate volcanism. J. Asian Earth Sci. 60, 88–103.
Wei, W., Zhao, D., Xu, J., Wei, F., Liu, G., 2015. P and S wave tomography and anisotropy in Northwest Pacific and East Asia: constraints on stagnant slab and intraplate volcanism. J. Geophys. Res. Solid Earth 120, 1642–1666.
Wei, W., Hammond, J., Zhao, D., Xu, J., Liu, Q., Gu, Y., 2019. Seismic evidence for a mantle transition zone origin of the Wudalianchi and Halaha volcanoes in Northeast China. Geochem. Geophys. Geosyst. 20, 398–416.
Xu, Y.G., 2007. Diachronous lithospheric thinning of the North China Craton and formation of the Daxin'anling-Taihangshan gravity lineament. Lithos 96, 281–298.
Xu, J., Liu, G., Wu, J., Ming, Y., Wang, Q., Cui, D., Shangguan, Z., Pan, B., Lin, X., Liu, J., 2012. Recent unrest of Changbaishan volcano, Northeast China: a precursor of a future eruption? Geophys. Res. Lett. 39, L16305. https://doi.org/10.1029/2012GL052600.
Xu, J., Pan, B., Liu, T., Hajdas, I., Zhao, B., Yu, H., Liu, R., Zhao, P., 2013. Climatic impact of the millennium eruption of Changbaishan volcano in China: new insights from high-precision radiocarbon wiggle-match dating. Geophys. Res. Lett. 40, 54–59. https://doi.org/10.1029/2012GL054246.
Xu, Y.G., Li, H., Hong, L., Ma, L., Ma, Q., Sun, M., 2018. Generation of Cenozoic intraplate basalts in the big mantle wedge under eastern Asia. Sci. China Earth Sci. 61, 869–886.
Xu, W., Chen, J., Wang, A., Tang, J., Wang, F., Wang, C., Guo, P., Wang, Y., Yang, H., Sorokin, A., 2021. Stagnant slab front within the mantle transition zone controls the formation of Cenozoic intracontinental high-Mg andesites in northeast Asia. Geology 49, 19–24. https://doi.org/10.1130/G47917.1.
Yan, D., Tian, Y., Zhao, D., Li, H., 2023. Seismicity and magmatic system of the Changbaishan intraplate volcano in East Asia. J. Geophys. Res. Solid Earth 128. https://doi.org/10.1029/2023JB026853 e2023JB026853.
Yang, J., Faccenda, M., 2020. Intraplate volcanism originating from upwelling hydrous mantle transition zone. Nature 579, 88–91.
Ye, L., Li, J., Tseng, T., Yao, Z., 2011. A stagnant slab in a water bearing mantle transition zone beneath Northeast China: implications from regional SH waveform modeling. Geophys. J. Int. 186, 706–710.

Zhang, C., Zhang, X., Zhao, J., Liu, B., 2002. Crust-mantle structure of the Changbaishan Tianchi volcanic area and its vicinity: an exploratory study and its implications. Chin. J. Geophys. 45, 862–871.
Zhang, M., Guo, Z., Sano, Y., Cheng, Z., Zhang, L., 2015. Stagnant subducted Pacific slab-derived CO2 emissions: insights into magma degassing at Changbaishan volcano, NE China. J. Asian Earth Sci. 106, 49–63.
Zhang, M., Guo, Z., Liu, J., Liu, G., Zhang, L., Lei, M., Zhao, W., Ma, L., Sepe, V., Ventura, G., 2018. The intraplate Changbaishan volcanic field (China/North Korea): a review on eruptive history, magma genesis, geodynamic significance, recent dynamics and potential hazards. Earth Sci. Rev. 187, 19–52.
Zhang, R., Brenna, M., White, J., Kereszturi, G., 2024a. Variable controlling factors lead to contrasting patterns of volcanism in the Changbaishan volcanic area (Tianchi-Longgang), China-North Korea: insights from morphometry and spatial-temporal analyses. J. Volcanol. Geotherm. Res. 451, 108116.
Zhang, Z., Deng, Y., Xu, Y., Li, X., 2024b. A translithospheric magmatic system revealed beneath Changbaishan volcano. Geology 52, 742–746.
Zhao, D., 2004. Global tomographic images of mantle plumes and subducting slabs: insight into deep earth dynamics. Phys. Earth Planet. Inter. 146, 3–34.
Zhao, D., 2015. Multiscale Seismic Tomography. Springer, 304 pp.
Zhao, D., 2021. Seismic imaging of Northwest Pacific and East Asia: new insight into volcanism, seismogenesis and geodynamics. Earth Sci. Rev. 214, 103507.
Zhao, D., Tian, Y., 2013. Changbai intraplate volcanism and deep earthquakes in East Asia: a possible link? Geophys. J. Int. 195, 706–724.
Zhao, D., Hasegawa, A., Horiuchi, S., 1992. Tomographic imaging of P and S wave velocity structure beneath northeastern Japan. J. Geophys. Res. 97, 19909–19928.
Zhao, D., Lei, J., Tang, R., 2004. Origin of the Changbai intraplate volcanism in Northeast China: evidence from seismic tomography. Chin. Sci. Bull. 49, 1401–1408.
Zhao, D., Maruyama, S., Omori, S., 2007. Mantle dynamics of western Pacific to East Asia: new insight from seismic tomography and mineral physics. Gondwana Res. 11, 120–131.
Zhao, D., Tian, Y., Lei, J., Liu, L., Zheng, S., 2009. Seismic image and origin of the Changbai intraplate volcano in East Asia: role of big mantle wedge above the stagnant Pacific slab. Phys. Earth Planet. Inter. 173, 197–206.
Zhao, D., Pirajno, F., Dobretsov, N., Liu, L., 2010. Mantle structure and dynamics under East Russia and adjacent regions. Russ. Geol. Geophys. 51, 925–938.
Zhao, D., Yanada, T., Hasegawa, A., Umino, N., Wei, W., 2012. Imaging the subducting slabs and mantle upwelling under the Japan Islands. Geophys. J. Int. 190, 816–828.
Zhao, D., Fujisawa, M., Toyokuni, G., 2017. Tomography of the subducting Pacific slab and the 2015 Bonin deepest earthquake (Mw 7.9). Sci. Rep. 7, 44487. https://doi.org/10.1038/srep44487.
Zhao, L., Hu, Y., Zhan, Y., Sun, X., Wang, Q., Zhu, Y., Cao, C., 2022. Three-dimensional electrical structure and magma system of the monogenetic Longgang volcanic field, Northeast China, inferred from broadband magnetotelluric data. J. Geophys. Res. Solid Earth 127, e2022JB024694.
Zhao, D., Liu, X., Wang, Z., Gou, T., 2023a. Seismic anisotropy tomography and mantle dynamics. Surv. Geophys. 44, 947–982.
Zhao, D., Wang, J., Huang, Z., Liu, X., Wang, Z., 2023b. Seismic anisotropy and geodynamics of the East Japan subduction zone. J. Geodyn. 156, 101975.
Zhao, D., Liang, X., Toyokuni, G., Hua, Y., Xu, Y., 2024a. Cause of enigmatic upper-mantle earthquakes in Central Wyoming. Seismol. Res. Lett. 95, 2497–2505.
Zhao, L., Zhan, Y., Kiyan, D., Xu, J., Hu, Y., Tang, J., Sun, X., Wang, Q., Cao, C., 2024b. Magnetotelluric evidence for the deep causes of different eruptive styles of Changbaishan Tianchi and Longgang volcanoes. Sci. Rep. 14, 24897.
Zhu, R., Sun, W., 2021. The big mantle wedge and decratonic gold deposits. Sci. China Earth Sci. 64, 1451–1462.
Zhu, H., Tian, Y., Zhao, D., Li, H., Liu, C., 2019. Seismic structure of the Changbai intraplate volcano in NE China from joint inversion of ambient noise and receiver functions. J. Geophys. Res. Solid Earth 124, 4984–5002.